https://doi.org/10.1016/j.engstruct.2021.113682
This is the Pre-Published Version.

Prediction of residual stresses in high-strength S690 cold-formed square hollow sections using integrated numerical simulations

[a,b] Xiao M., [a,b] Hu Y.F., [a,b] Jin H., [a,b] Chung K.F.*, and [a,b,c] Nethercot D.A.

[a] Department of Civil and Environmental Engineering,
The Hong Kong Polytechnic University, Hong Kong SAR, China.

[b] Chinese National Engineering Research Centre for Steel Construction (Hong Kong Branch),
The Hong Kong Polytechnic University, Hong Kong SAR, China.

[c] Department of Civil and Environmental Engineering, Imperial College London, U.K.

* Corresponding author: *kwok-fai.chung@polyu.edu.hk*

Abstract

In general, residual stresses are induced in structural members during various fabrication processes, such as welding, bending, press-braking, folding, flame cutting and punching. The presence of those residual stresses in cold-formed square hollow sections (CFSHS) primarily caused by i) transverse bending (or cold-forming), and ii) longitudinal welding, is widely considered to have modified both initial stress and strain conditions of these steel members significantly. Hence, these residual stresses are widely considered to have significant adverse effects onto the structural performance of these CFSHS under various actions.

In order to examine and quantify both magnitudes and distributions of these residual stresses in S690 CFSHS, an investigation is undertaken to measure residual stresses due to transverse bending and longitudinal welding. Moreover, an approach of integrated numerical simulations is adopted in which a total of three co-ordinated finite element models are established together with various element types and block data transfers to generate compatible meshes for the following three analyses: i) two-dimensional plane-strain bending analyses with large plastic

deformations and springback, ii) three-dimensional heat transfer analyses for transient temperature distributions under a heat source, and iii) three-dimensional thermomechanical analyses for welding-induced residual stresses.

The predicted results of these three analyses have been carefully calibrated against various experimental data, such as surface temperatures during welding, and residual stresses and strains after welding. Good comparisons between the measured and the predicted data of these S690 CFSHS are demonstrated. The complete residual stress distributions within typical S690 CFSHS due to transverse bending and longitudinal welding are illustrated in three-dimensional plots while simplified residual stress patterns of these sections with specific values and parameters are also provided for subsequent advanced structural analyses and design.

The proposed modelling technique for transverse bending and longitudinal welding with compatible meshes of two-dimensional and three-dimensional models with various element types and block data transfers is demonstrated to be highly effective. The technique is readily applicable to simulate residual stresses of all fabricated sections manufactured with transverse bending and longitudinal welding, and, thus, the simulated residual stresses can be employed in subsequent structural analyses of all fabricated members.

Keywords:

High strength steel; cold-formed square hollow section; residual stress; numerical simulation; experimental investigation.

Notations

t	plate thickness (mm)
B	section width (mm)
H	section height (mm)
R_{in}	inner radius (mm)
L	member length (mm)
R_p	punch radius (mm)
S	stroke (mm)
β	initial corner angle (°)
$\Delta\beta$	springback angle (°)
β'	Final corner angle (°)
I	current (A)
U	voltage (V)
v	welding speed (mm/s)
η	welding efficiency
E	Young's modulus (kN/mm^2)
f_y	yield strength (N/mm^2)
f_u	tensile strength (N/mm^2)
ε	strain (%)
ε_L	strain at elongation limit (%)
PEEQ	equivalent plastic strain (%)
$\sigma_{res,t}$	tensile residual stress (N/mm^2)
$\sigma_{res,c}$	compressive residual stress (N/mm^2)

q_1	the power density in the front ellipsoid
q_2	the power density in the rear ellipsoid
q	linear heat input energy (kJ/mm)
f_1	the portion of the heat deposited in the front ellipsoid
f_2	the portion of the heat deposited in the rear ellipsoid
a_1	the length of the semi-axis along x-axis in the front ellipsoid (mm)
a_2	the length of the semi-axis along x-axis in the rear ellipsoid (mm)
b	the length of the semi-axis along y-axis (mm)
c	the length of the semi-axis along z-axis (mm)
U_x	the degree of freedom for translation along x-axis
U_y	the degree of freedom for translation along y-axis
U_z	the degree of freedom for translation along z-axis
ε_t	tensile residual strain (%)
ε_c	compressive residual strain (%)
F_T	total tension force (kN)
F_C	total compression force (kN)
F_R	resultant force (kN)
f_r	force ratio

1 Introduction

Nowadays, high strength structural steels are commonly produced in many modern steel mills in different parts of the world for a wide range of engineering applications, for examples, large lifting equipment in ports and mines, tower cranes and wind turbines. The term 'high strength steel' is generally used to describe structural steels with yield strengths equal to or larger than 690 N/mm^2, i.e. S690 steels, and hence, their yield strengths are almost double of those common structural S355 steels with yield strengths at 355 N/mm^2. With recent advances in steel-making technology and equipment, these high strength S690 steels are produced with carefully controlled heating / cooling processes, namely, i) a quenching and tempering process, or ii) a thermomechanical controlled process. These processes are devised and implemented in industrial scales to produce specific microstructures to attain various mechanical properties with minimum materials, equipment and energy costs. S690 steel plates are commonly produced within a thickness range of 6 to 80 mm to various steel material specifications, such as ASTM A514 (ASTM 2018), EN 10025-6 (CEN 2019a) and GB/T 1591 (CNS 2018).

Many engineers are very interested in exploiting potential uses of these S690 steels in construction in order to reduce self-weights of structural members significantly. Through various fabrication procedures, such as cutting, bending (or folding) and welding, fabricated sections are produced as structural members with a wide range of shapes and sizes. Owing to high structural efficiency, cold-formed structural hollow sections are popular structural members as they possess large cross-section resistances, and they have a reduced tendency towards instability. Hence, cold-formed square hollow sections (CFSHS) and circular hollow sections (CFCHS) made of high strength S690 steels are considered to be highly efficient

members to be used in heavily loaded and long-span structures. Hence, there is a clear need to examine the structural behaviour of these high strength S690 CFSHS and CFCHS. It should be noted that an accurate description on the residual stresses in these fabricated sections is important to examine their structural behaviour under various loading conditions. Therefore, it is essential to develop a scientific method to quantify both the magnitudes and the distributions of the residual stress patterns induced during fabrication, i.e. i) transverse bending, and ii) longitudinal welding.

1.1 Residual stresses in cold-formed structural hollow sections

Residual stresses are inevitably induced in structural members and joints by transverse bending and longitudinal welding during fabrication. These residual stresses in structural members tend to cause pre-mature yielding in the steel, and hence, adversely affect their overall structural performance under various actions. It is important to allow for the presence of these residual stresses in structural design of these fabricated sections, so that any reduction in the cross-section resistances of these fabricated sections as well as their member resistances have been properly accounted for. Typical residual stress patterns are given in ECCS (1986), as shown in Fig. 1, and these patterns are commonly employed in structural design of hot-rolled H-sections and hollow sections as well as welded sections of S235 to S355 steels. It should be noted that applications of these residual stress patterns to S690 CFSHS and CFCHS are somehow uncertain because of a significant increase in the yield strength, i.e. from 355 to 690 N/mm^2, as the effects of residual stresses are expected to be proportionally less pronounced in the structural behaviour of these S690 sections according to Ma et al. (2018), Liu and Chung (2018) and Liu et al. (2019).

1.2 Experimental measurements on residual stresses

In general, both the magnitudes and the distributions of these residual stresses should be systematically examined in order to determine how these residual stresses will affect the structural behaviour of structural members and joints. There are three measurement methods on residual stresses (Withers and Bhadeshia 2001; Rossini et al. 2012), namely, i) destructive methods, ii) semi-destructive methods, and iii) non-destructive methods. In both the destructive and the semi-destructive methods, the residual stresses are measured through complete or partial stress relief after removing materials. These methods rely on the deformations upon local removal of materials from the steel plates, and hence, releases of the residual stresses. Thus, both the sectioning method and the hole-drilling method are representatives of the destructive and the semi-destructive methods, respectively. However, it should be noted that:

a) The measured results of the sectioning method are often found to vary significantly, as reported by various researchers (Ban et al. 2012; Wang et al. 2012; Ban et al. 2013a; Ban et al. 2013b; Li et al. 2015; Ma et al. 2015; Yang et al. 2017; Somodi and Kövesdi et al. 2017; Somodi and Kövesdi et al. 2018; Chen and Chan 2020; Hu et al. 2020), owing to various operational problems in practice. In many cases, the measured residual stresses within a fabricated section are found not to be in equilibrium, i.e. the total tension force within the section is not equal or even close to the corresponding compression force. Hence, there is some concern on accuracy of the results of the sectioning method despite it is widely adopted in many experimental studies.

b) While the hole-drilling method is considered to be able to give precise surface residual stresses on flat portions of fabricated sections, it is not able to work on curved portions or internal surfaces of some of these sections due to practical access problems (Lee et al. 2012a; Lee et al. 2014a; Yang et al. 2017; Liu and Chung 2018). Hence, additional numerical data are often needed to establish a complete picture on the residual stress distributions within the sections.

It should be noted that the non-destructive methods measure physical parameters related to stresses in the steel sections with no damage throughout the measuring processes. Among non-destructive methods, the neutron diffraction method is a representative one, which measures the differences in the lattice spacings between a stressed specimen and a stress-free reference specimen, thus, to determine the residual stresses (Khan et al. 2016). However, many researchers are not able to have regular access to an equipment of this method in practice.

As reported in the literature, the residual stress measurements in high strength welded sections have been conducted by many researchers. Table 1 summarizes a number of experimental investigations into high strength steel welded sections reported in the past decade, and these investigations cover many different steels with yield strengths ranging from 420 to 1100 N/mm^2. Among these investigations, the residual stresses in various types of fabricated sections are examined, including folded angles, plate-to-plate joints, T-joints, H-sections, I-sections, box-sections as well as cold-formed circular, square and rectangular sections. It is found that the effects of residual stresses in high strength welded sections are typically less severe than those observed in similar sections of common strength steel reported in the literature.

1.3 Numerical simulation on residual stresses

Welding is a widely adopted process in steel fabrication to join steel plates and sections together. High quality metal, in the form of welding electrodes, are heated up, by a steady supply of electricity, to become molten weld metal which is then deposited along the welding seams of the steel plates. According to the transient temperatures of the molten weld metal, the steel plates expand quickly, and then, contract according to various thermal properties and physical arrangements of the welding seams. Owing to differential transient temperatures within the welding seams during cooling, residual stresses are induced.

In order to investigate the effects of welding onto the welded sections, coupled thermomechanical analyses are widely employed to simulate both the processes of heating up of the welded sections during welding, and then cooling down of the welded sections after welding. It should be noted that both the temperature history and the residual stresses of welded sections are commonly predicted with the use of a double-ellipsoidal heat source model as proposed by Goldak et al. (1984).

Over the past three decades, a number of heat source models were developed by a number of researchers to simulate heat transfer during welding. Nguyen et al. (1999) proved applicability of his proposed model in a semi-infinite body, but this was only correct when the front and the rear ellipsoids were equal. The model was further developed by Fachinotti et al. (2011) to achieve improved accuracy, and the newly proposed analytical solution was shown to be applicable to the problem of unsteady thermal conduction in a semi-infinite medium. However, such an improvement on accuracy of the heat source model was found to have only minor

improvements on prediction of the residual stresses. In general, the researchers in the international research community of steel structures tend to employ the original double-ellipsoidal model, i.e. the simple one proposed in 1984, for analyses of the residual stresses.

As reported in the literature, the model has been successfully employed in various numerical investigations into the residual stresses of high strength steel welded sections. Lee et al. (2012b and 2014b) employed the heat source model to simulate the residual stresses in high strength steel plate-to-plate joints. The corresponding numerical models were carefully validated, and they were shown to be able to predict accurate residual stresses under the given conditions of welding. The same heat source model was also employed by Jiang et al. (2017). It was demonstrated that numerical predictions were successfully achieved in high strength steel box-sections with two different finite element packages.

In the recent years, a number of investigations on various advanced topics, such as, heat source model, plasticity constitutive model and phase transformation, were reported in the literature, and phase transformation is considered to be a major concern (Ni et al. 2020). Alhafadhi and Krallics (2020) investigated welding-induced residual stresses in carbon steels through numerical simulation, and phase transformation was incorporated. It was demonstrated that the residual stresses in low carbon steels were not affected by phase transformation while those in high carbon steels were considerably affected by martensitic transformation. Zhang et al. (2021) considered bainite transformation in his numerical simulation on welding S355J2 steel, and both the magnitudes and the distributions of residual stresses were examined. Good agreement between the numerical and the experimental results indicated that the undercooling austenite

and the bainitic transformation strains were crucial for predicting accurate residual stresses in heat-affected zones. Tankova et al. (2019) successfully predicted the residual stresses in S355 welded I-sections with a traditional three-dimensional thermomechanical model, and good agreements between the overall numerical and the experimental results were established.

1.4 Relevant investigations on residual stresses by the authors

It should be noted that a systematic numerical investigation into the residual stresses in high strength S690 steel welded H-sections was conducted by Liu and Chung (2018). The proposed thermomechanical models were well calibrated against various measurements on the surface residual stresses obtained with the hole-drilling method, and the models were capable of accurately predicting the temperature history as well as the residual stresses in S690 welded H-sections. The validated models were then employed to carry out a parametric study to assess the effects of steel grades, numbers of welding passes and heat input energy onto the residual stresses in S690 welded H-sections (Liu et al. 2019). It was found that the residual stresses in these S690 welded H-sections were proportionally smaller than those in S355 welded H-sections. The effects induced by welding passes with different heat input energy onto the residual stresses were also well demonstrated.

Moreover, an experimental and numerical investigation into the effects of residual stresses onto the structural behaviour of T-joints between S690 cold-formed circular hollow sections was conducted and reported by the authors (Hu et al. 2020). Advanced finite element models with sequentially-coupled thermomechanical analyses were performed to assess the effects of welding-induced residual stresses at the brace / chord junctions onto structural behaviour of

these T-joints under brace in-plane moments. The effects of these residual stresses are demonstrated to be significantly less pronounced than those anticipated, and hence, the structural behaviour of these T-joints is found not to be significantly affected by these residual stresses.

2 Objectives and scope of work

In general, residual stresses are induced in structural members during various fabrication processes, such as welding, bending, press-braking, folding, flame cutting and punching. The presence of these residual stresses is widely considered to cause significant modifications to the initial stress and strain conditions of these steel members, and often, reductions to their structural performance under various actions.

In order to examine and quantify both magnitudes and distributions of these residual stresses in S690 CFSHS, an investigation was undertaken to measure residual stresses due to transverse bending and longitudinal welding. Moreover, an approach of integrated numerical simulations is adopted in which a total of three co-ordinated finite element models are established together with various element types and block data transfers to generate compatible meshes for the following three analyses: i) two-dimensional (2-D) plane-strain bending analyses with large plastic deformations and springback, ii) three-dimensional (3-D) heat transfer analyses for transient temperature distributions under a heat source, and iii) three-dimensional (3-D) thermomechanical analyses for welding-induced residual stresses. Fig. 2 presents a flowchart on the integrated numerical simulations on residual stresses induced in these S690 CFSHS during fabrication. The predicted results of these three analyses have been carefully calibrated

against various experimental data obtained from systematic measurements, such as surface temperatures during welding, and residual stresses after welding. Table 2 summarizes the activities conducted in the present investigation.

The following areas of interest are examined thoroughly:

a) Accuracy of both the thermal and the thermomechanical models in predicting transient surface temperatures and surface residual stresses distributions in the S690 CFSHS.

b) Residual stresses due to i) transverse bending, and ii) longitudinal welding, and their combined stress distributions in the S690 CFSHS.

c) Modelling technique for transverse bending and longitudinal welding with compatible meshes of two-dimensional and three-dimensional models with various element types and block data transfers.

2.1 Fabrication of cold-formed square hollow sections

Fig. 3 illustrates the geometry of four CFSHS of S690 steels covered in the current investigation:

i) Sections S1-R and S1-S, both with plate thickness at 6 mm, and

ii) Sections S3-R and S3-S, both with plate thickness at 10 mm.

In general, Section R is made with a pair of cold-bent C-sections, and their free edges are welded up to form a square hollow section. Hence, there are 4 round corners and 2 welding seams, and such a fabrication method is commonly adopted. However, Section S is fabricated differently. A single cold-bent U section with 2 round corners is made, and its free edges are

welded onto a flat plate to form a square hollow section. As there are only 2 round corners and 2 welding seams, there is a potential saving in the fabrication effort. Typical fabrication processes of CFSHS are:

a) Transverse bending

The steel plates are cut to sizes, and a punch and two supports are adopted which radii are assigned to be equal to 3 x plate thickness. Hence, through a trial-and-error process, the stroke of the punch is selected so that the steel plate is bent to achieve a round corner with internal angle at 90^{o} after elastic springback.

b) Longitudinal welding

After a careful alignment, the free edges of both the bent sections are welded together with a Gas Metal Arc Welding (GMAW) method by a qualified welder. The welding procedures are established with specific ranges of welding parameters for both 6 and 10 mm thick steel plates, as summarized in Table 3. With a proper control on the welding process, no reduction in the mechanical properties of the welded sections is expected according to experiences on previous projects on S690 welded H- and I-sections.

All the cold-formed square hollow sections are fabricated in a well equipped fabrication yard. It should be noted that the lengths of Sections S1-R and S1-S are 560 mm while those of Sections S3-R and S3-S are 760 mm. As the lengths of these sections are larger than three times of their widths, the residual stresses induced by both transverse bending and longitudinal welding are assumed to be distributed uniformly over the central portions of the sections. Hence,

measurements made at the central portions of the sections are unlikely to be affected by end effects.

2.2 Key mechanical properties of the S690 steel plates

Standard coupons were extracted from the S690 CFSHS according to BS EN ISO 6892-1 (CEN 2019b), and standard tensile tests were conducted successfully also according to BS EN ISO 6892-1 with a proper control on the straining rates of the coupons. Table 4 summarizes key mechanical properties of both flat and curved coupons of the S690 CFSHS.

3 Numerical Investigation

In the present investigation, a total of three finite element models are established using the general finite element package Abaqus (2013) together with various element types and block data transfers to generate compatible meshes for the following analyses:

a) Transverse bending

Transverse bending is a mechanical process in which steel plates are bent with a punch to form round corners. This process is readily simulated with a two-dimensional (2-D) stress model to perform plastic deformation analyses of the steel plates with two-dimensional plane-strain element CPE4R. The model is specifically devised to undergo large plastic deformations to simulate highly localized transverse bending of the steel plates through the relative stroke of the punch and its supports, followed with an elastic springback.

b) Longitudinal welding

Welding is a thermomechanical process as molten electrodes at about 1350 to 1500 ºC are deposited onto prepared edges of the steel plates in a controlled manner. Obviously, the edges of the steel plates are quickly heated up, and then, gradually cooled down according to various welding processes, procedures and parameters. These edges expand quickly during welding, and then contract gradually after welding, and hence, residual stresses are induced within the welded joints owing to differential contraction. Hence, in order to simulate the process, two finite element models with sequential analyses are developed, namely, i) a three-dimensional (3-D) thermal model with heat transfer element DC3D8, and ii) a three-dimensional (3-D) thermomechanical model with stress element C3D8R.

It is important to use a properly calibrated heat source to represent the welding arc so that the heat input energy during welding is accurately simulated to determine the transient temperature distribution of the model during welding. Based on various codified thermal properties at elevated temperatures, both the thermal and the mechanical responses of the welded joints are properly simulated, and the induced residual stresses within the welded joints are then predicted according to the transient temperature distributions.

Owing to large quantities of data to be transferred among the three co-ordinated numerical models, a simple programme was developed to perform the following:

i) to extract residual stresses computed from the two-dimensional plane-strain bending model, and then, to incorporate these residual stresses onto the three-dimensional thermomechanical model; it should be noted that it is necessary to consolidate these

residual stresses of up to 100 layers across the thicknesses in the plane-strain bending models into residual stresses of up to 6 layers in the thermomechanical model;

ii) to extract transient temperature distribution history computed from the three-dimensional heat transfer model, and then, to incorporate these temperature data onto the three-dimensional thermomechanical model; and

iii) to extract residual stresses computed from the three-dimensional thermomechanical model, and then, to incorporate these residual stresses onto the three-dimensional structural model for subsequent analyses.

Hence, these block data transfers are able to ensure data compatibility among these three models, and facilitate numerical analyses with a high degree of data accuracy.

3.1 Simulation of transverse bending

As shown in Fig. 3, Sections S1-R and S3-R are fabricated with two different plate thicknesses, namely, 6 and 10 mm thick, while their inner radius to thickness ratio, R_{in} / t , is specified to be 3.0. Hence, two-dimensional transverse bending models for the cold-bent corners of both Sections have been established, and Fig. 4 illustrates the two-dimensional transverse bending model for the cold-bent corner of Section S1-R.

3.1.1 Finite element model and mesh convergence study

As transverse bending is a well-defined plane-strain problem, the steel plate is modelled as a deformable body with the commonly used plane-strain element CPE4R while the punch and the two supports are modelled as rigid bodies. The radii of both the punch and the supports, R_p

and R_s , are assigned to be 3 x t where t is the plate thickness. Interaction surfaces are set between the pairs of the contact surfaces to enable friction between the punch and the plate as well as that between the plate and the supports. While the supports are fixed throughout the bending process, the punch travels a vertical distance, i.e. the stroke, S , to impose a bending action onto the plate. Hence, the plate is progressively bent until its inner radius reaches R_p . Then, the punch is removed, and all the interactions are released so that springback occurs freely in the plate. Hence, a compensation to the springback angle, $\Delta\beta$, should be allowed for in the initial corner angle, β , and a trial-and-error process is performed to determine the magnitude of the stroke, S , in order to obtain the final corner angle, β' (or $\beta + \Delta\beta$), to be as close as possible to 90°. It should be noted that the final magnitudes of the strokes S adopted for bending 6 and 10 mm plates are 33.7 and 50.5 mm respectively.

In order to establish numerical convergence, a total of three meshes with different element sizes are established as follows:

a) Mesh TB20

b) Mesh TB50, and

c) Mesh TB100

It should be noted that the aspect ratio of all the CPE4R plane-strain elements adopted in the models is 1:1, and key parameters of these meshes are summarized in Table 5.

After successful analyses of these three models with different meshes, the contours of equivalent plastic strains PEEQ of these models were plotted onto the deformed meshes shown

in Fig. 5 a). It is shown that these contours in the vicinity of the round corners are very similar to one another. Moreover, the cross-sectional variations of the PEEQ, and both the longitudinal and the transverse residual stresses of these three meshes are plotted in Fig. 5 b) for a direct comparison. It is apparent that convergence of each of these variations is attained. Owing to an increase in the compression area above the mid-plane surface as well as a corresponding decrease in the tension area below the surface, the neutral surface is found to be shifted above the mid-plane surface. There is an abrupt change in the stresses in the vicinity of the neutral surface, and hence, a highly localized mesh refinement is provided there.

3.1.2 Residual stresses due to transverse bending

Fig. 6 illustrates the cross-sectional plots of the longitudinal residual stresses of the cold-bent corners of both Sections S1-R and S3-R induced after transverse bending, and it is apparent that these stress plots are very similar to one another. In order to incorporate these residual stresses into the three-dimensional finite element models for subsequent analyses, it is necessary to consolidate these stresses across the thicknesses into only a small number of layers to achieve a high computational efficiency. It is shown that:

- As the plate thickness of Sections S1-R and S1-S is 6 mm, there are 3 layers of solid elements in the three-dimensional models. Hence, all these residual stresses are consolidated into merely 3 layers of stresses.

- Similarly, as the plate thickness of Sections S3-R and S3-S is 10 mm, there are 4 layers of solid elements in the three-dimensional models. Hence, all these residual stresses are

consolidated into merely 4 layers of stresses.

These consolidated residual stresses are then incorporated into the three-dimensional thermomechanical models through a block data transfer as initial stresses for subsequent thermomechanical analyses to provide residual stress distributions in these CFSHS.

3.2 Simulation of longitudinal welding

As shown in Fig. 2, a rational simulation of longitudinal welding comprises of the following two sequential non-linear analyses:

i. Three-dimensional heat transfer analysis

A three-dimensional thermal model is established to determine temperature history of the steel plates during and after welding, and three-dimensional heat transfer element DC3D8 is employed in the model. It is important to use a properly calibrated heat source to represent the welding arc so that the heat input energy during welding is accurately simulated to determine the transient temperature variations of the model due to welding.

ii. Three-dimensional thermomechanical analysis.

A three-dimensional thermomechanical model is also established to determine mechanical responses of the steel plates under the effects of transient temperature variations due to welding, and three-dimensional stress element C3D8R is adopted. Based on the predicted temperature history obtained from above, the mechanical responses of the model under the temperature variations, i.e. the heating up phase during welding, and then, the cooling

down phase after welding, locked-in stresses due to differential cooling and contraction is determined.

It should be noted that both the three-dimensional models for heat transfer analyses and thermomechanical analyses are fully compatible so that the temperature data predicted in the thermal model are readily transferred into the thermomechanical model. Both the welding parameters and the transient temperature variations of the Sections shown in Fig. 3 are recorded throughout the entire course of welding while residual stresses in these Sections are measured with the sectioning method. Hence, these measured data are readily adopted for careful calibration of these models.

3.2.1 Thermal and mechanical properties of materials

During welding, the steel plates go through quick changes in temperatures with large gradients. It is important to specify how the thermal properties of the steel plates vary with temperatures during welding because these properties define how the steel plates behave both physically and numerically. EN 1993-1-2 (CEN 2009) provides a set of reduction factors for temperature-dependent thermomechanical properties for S235 to S460 steels at elevated temperatures, namely, thermal conductivity, specific heat capacity, thermal expansion coefficient as well as yield strength and Young's modulus. However, as there are only limited studies on these temperature-dependent thermal properties of the high strength S690 steels, it is considered to be acceptable to employ these reduction factors in EN 1993-1-2 in both the heat transfer and the thermomechanical analyses for the high strength S690 steels in the present investigation, as recommended in EN 1993-1-12 (CEN 2007). The reduction factors for both the yield

strength and the Young's modulus are illustrated in Fig. 7.

Fig. 8 illustrates the true stress-strain curves of both the 6 and the 10 mm thick S690 steel plates based on the standard tensile tests, and hence, the key mechanical properties, reported in Section 2.2. By adopting the reduction factors mentioned above, the true stress-strain curves of the steel plates at elevated temperatures are readily incorporated into the models.

It should be noted that the same sets of codified thermal and mechanical properties together with reduction factors of the steel plates are also adopted as those of the weld metal as an over-match electrode is assumed to be employed in welding. In general, the heat input energy during welding in the present study is kept to be low in order to prevent any significant phase transformation in the heat affected zones of the S690-QT steel according to previous experiences (Ma et al. 2018; Liu et al. 2018). For further information on microstructural evolution of the S690-QT steel after welding, refer to Ho et al. (2020).

3.2.2 Double-ellipsoidal heat source model

A double-ellipsoidal model widely adopted for simulation of a heat source for arc welding is illustrated in Fig. 9 together with various parameters to define its dimensions. The two normal distributions, i.e. one in the front ellipsoid and the other one in the rear ellipsoid, of the heat fluxes are presented along the x-axis.

$$q_1\,(x,y,z,t) \;=\; \frac{6\sqrt{3}f_1 q}{a_1 bc\pi\sqrt{\pi}}\; exp(-\frac{3(x-vt)^2}{a_1^2})\; exp(-\frac{3y^2}{b^2})\; exp(-\frac{3z^2}{c^2}) \qquad \text{Eq. (1)}$$

$$q_2\,(x,y,z,t) = \frac{6\sqrt{3}f_2 q}{a_2 bc\pi\sqrt{\pi}}\, exp(-\frac{3(x-vt)^2}{a_2^2})\, exp(-\frac{3y^2}{b^2})\, exp(-\frac{3z^2}{c^2}) \qquad \text{Eq. (2)}$$

where

q_1 (x, y, z, t) is the power density in the front ellipsoid;

q_2 (x, y, z, t) is the power density in the rear ellipsoid;

q is the linear heat input energy (kJ/mm);

f_1 is the portion of the heat deposited in the front ellipsoid;

f_2 is the portion of the heat deposited in the rear ellipsoid; and

a_1, a_2, b and c are the lengths of the semi-axes (mm).

3.2.3 Finite element models

Fig. 10 illustrates the finite element models of both Sections S3-R and S3-S together with the boundary conditions for the heat transfer and the thermomechanical analyses. In general, the boundary conditions of these two Sections are similar. At one end of the Sections, the degrees of freedom for translation in all the three directions are fixed, i.e. $U_x = U_y = U_z = 0$. At the other end of the Sections, the degrees of freedom for translation in the cross-sectional plane of the Sections are fixed, i.e. $U_y = U_z = 0$. Hence, all the Sections are able to expand along their longitudinal direction freely during welding.

3.2.4 Multi-pass welding

In order to prevent microstructural changes in the S690 steel plates, it is important to control the amount of heat input energy during welding (Liu and Chung 2018; Liu et al. 2019; Hu et a. 2020). Hence, multi-pass welding is adopted during the welding of all these Sections. Fig. 11

illustrates the modelling of various multi-pass welding processes in all the four Sections, and the sequences of various welding passes for the welded joints of Sections S1-R and S3-R, and also of Sections S1-S and S3-S are fully illustrated. It should be noted that:

- As shown in Fig.11 a), Passes T1 and T2 are performed sequentially at the top of Section S1-R while Passes B1 and B2 are performed sequentially at the bottom of the Section. Similarly, as shown in Fig. 11 b), Passes T1, T2 and T3 are performed sequentially at the top of Section S3-R while Passes B1, B2 and B3 are performed sequentially at the bottom of the Section. Passes T3 and B3 are required in Section S3-R because of its increased thickness at 10 mm, when compared with that of Section S1-R at 6 mm.

- Similar arrangements on welding passes for Sections S1-S and S3-S are made as shown in Figs. 11 c) and d).

Owing to the mesh configurations of these welded joints, it is not practical to specify that the volumes deposited in various welding passes are the same. However, it should be noted that the welding parameters of each pass are summarized in Table 3, and they are the current, I, the voltage, U, the welding speed, v, and the welding efficiency, η. Based on these parameters, the linear heat input energy, q, of these welding passes are readily obtained. These welding parameters are very important to both the heat transfer and the thermomechanical analyses.

3.2.5 Mesh convergence study

In order to demonstrate convergence of the proposed finite element models, a mesh convergence study has been carried out on Section S3-R to identify a proper mesh configuration which achieves a balance between numerical accuracy and computational efficiency for both the heat transfer and the thermomechanical analyses of all four CFSHS. Fig. 12 illustrates the following models with different mesh configurations having different numbers of elements across the plate thickness:

- Mesh L03
- Mesh L04, and
- Mesh L06

The longitudinal residual stresses due to transverse bending shown in Fig. 6 are divided into the corresponding numbers of layers, and thus, incorporated into the corner regions of these three models with different mesh sizes. Fig. 13 illustrates various consolidated residual stresses adopted in the round corners of these three models. Both the heat transfer and the thermomechanical analyses on these three models have been performed successfully.

Fig. 14 illustrates the maximum transient temperature distributions of these three models during multi-pass welding while Fig. 15 illustrates the longitudinal residual strains of the models after welding. It is apparent that both the predicted temperatures and the predicted strains are highly similar among these three models.

Fig. 16 illustrates the predicted longitudinal residual strains on both the outer and the inner surfaces of Section S3-R evaluated with these three meshes. Since the Section is symmetrical,

the results of only half of the Section are presented, i.e. from Points A to A'. It should be noted that:

- For the maximum tensile residual strains $\varepsilon_{t,o,max}$ along the outer surface of the Section, the values of these three models are found to range from 0.379 to 0.391 %, and they occur in the vicinity of the welding seams.

- For the maximum compressive residual strains $\varepsilon_{c,i,max}$ along the inner surface of the Section, the values of these three models are found to range from -0.115 to -0.164 %, and they occur at the round corners.

Both the maximum tensile and the maximum compressive residual strains of these models are summarized in Table 6, and convergence of these values is evident among these three models. It is demonstrated that Mesh L06 is able to evaluate converged values of residual stresses at both the outer and the inner surfaces of the steel plates. In summary, after considering a balance between numerical accuracy and computational efficiency, Mesh L04 is adopted for subsequent analyses of both heat transfer and thermomechanical analyses of all the Sections covered in the present investigation.

3.2.5 Numerical results

A total of four models have been developed according to the dimensions of Sections S1-R and S1-S, and S3-R and S3-S, and Table 7 summarizes the details of the meshes of these models.

It should be noted that the aspect ratios of all the DC3D8 heat transfer elements and the C3D8R stress elements adopted in the models are 1:2:4 to minimize hour-glass effects during computation.

After a full incorporation of the welding parameters, the double-ellipsoidal model for the heat source of a welding arc is adopted in the heat transfer analyses while all the temperature-dependent thermal and mechanical properties of the steels are also incorporated into both the heat transfer and the thermomechanical analyses.

a) Heat transfer analyses

Based on various parameters of the welding processes summarized in Table 3, the proposed thermal models are analysed successfully, and various transient temperature distributions of the steel plates along the welding seams are determined according to the sequences of the welding passes presented in Fig. 11.

It should be noted that during welding, an infra-red camera was employed to record the surface temperature distribution history of the welded joints during each pass of the multi-pass welding of the Sections, as shown in Fig. 17. Hence, the measured and the predicted transient surface temperature history of both Sections S3-R and S3-S at a specific monitoring point 15 mm away from the centreline of the welding seams are plotted onto the same graphs in Fig. 18. It is shown that:

- For Section S3-R, the peak temperatures measured by the infra-red camera are 349, 346 and 484 °C during Passes T1, T2 and T3 respectively while the corresponding temperatures predicted by the proposed models are 306, 356 and 486 °C respectively.

- For Section S3-S, the peak temperatures measured by the infra-red camera are 259, 305 and 361 °C during Passes T1, T2 and T3 respectively while the corresponding temperatures predicted by the proposed models are 196, 304 and 437 °C respectively.

Thus, the predicted temperature curves of both Sections S3-R and S3-S are found to be in a good agreement with the corresponding measured curves. There was some irregularity in the measured temperatures after welding, and these were caused by blockage of the line of sight of the infra-red camera by the welder for various operations.

Hence, the proposed models have been demonstrated to be able to predict the transient surface temperatures of the Sections due to welding satisfactorily.

b) Thermomechanical analyses

It is important to establish the initial conditions of the proposed thermomechanical model in order to simulate the fabrication process of the CFSHS correctly as follows:

i. longitudinal residual stresses induced by transverse bending described in Section 3.1.2 should be incorporated into the round corners of the sections; and

ii. transient temperature distribution history predicted in the heat transfer analyses described above should also be incorporated into the vicinity of the welding seams of the sections.

These data have been incorporated into the thermomechanical model through block data transfer.

The proposed thermomechanical models have been analysed successfully, and residual strains induced during sequential thermal expansion and contraction in the welding seams were evaluated according to the thermal properties of the steel plates at elevated temperatures, i.e. thermal conductivity, specific heat capacity, linear thermal expansion coefficient, as shown in Fig. 7 a). Corresponding residual stresses and strains are then induced during simulation of the welding according to the mechanical properties of the steel plates, i.e. yield strength and Young's modulus at elevated temperatures, as shown in Fig. 7 b).

Fig. 19 illustrates typical details of the sectioning method, and residual stresses of these sections are determined with systematic analyses on measured surface strains before and after sectioning. The predicted longitudinal residual strains of Sections S3-R and S3-S are plotted in Figs. 20 and 21, and both the values along the outer and the inner surfaces of the sections are presented together with measured values obtained from the sectioning method for a direct comparison. It is shown that:

- Large residual tensile strains are found at both the inner and the outer surfaces of i) the welded seams of Section S3-R, and ii) the welded (sharp) corners of Section S3-S.

- Significant residual tensile and compressive strains are found at the outer and the inner surfaces respectively of the round corners of both Sections S3-R and S3-S.

In general, it is shown that good agreements between the predicted and the measured residual stresses at both the outer and the inner surfaces of the Sections are achieved.

c) Force equilibrium

In order to check force equilibrium at the Sections, the longitudinal forces developed within the entire cross-sections according to the predicted as well as the measured residual stresses are evaluated. Table 8 summarizes the total tension and the total compression forces, i.e. F_T and F_C respectively, within the sections as well as their resultant forces F_R together with the force ratios f_r which are given by $|F_R| / \Sigma \{|F_T| + |F_C|\}$. It is shown that:

- For Section S3-R

  i) The predicted resultant force F_R is found to be -34 kN while the corresponding force ratio of f_r is found to be 2.9 %.

  ii) The measured resultant force F_R is found to be -92 kN while the corresponding force ratio f_r is found to be 15.8 %.

- For Section S3-S

  i) The predicted resultant force F_R is found to be -15 kN while the corresponding force ratio f_r is found to be 1.5 %.

ii) The measured resultant force F_R is found to be -96 kN while the corresponding force ratio f_r is found to be 25.0 %.

Hence, it is evident that the residual stresses predicted by the proposed models are readily in equilibrium with an error of smaller than 3.0 %, when compared with those stresses measured with the sectioning methods.

It should be noted that the measured forces F_T and F_C are found to be very different to their corresponding predicted values. Moreover, both their resultant forces F_R and their force ratios f_r are very different to their corresponding predicted values. After a close examination on the measured data, it is suggested that the errors are mainly due to a significant under-estimation on all the residual strains, in particular, the residual tensile strains of the welds and also those strains in the vicinity of the welding seams. This agrees with the findings in similar research studies and previous experiences (Wang et al. 2012; Hu et al. 2020) on residual stress measurements with the sectioning method.

Fig. 22 illustrates the predicted longitudinal residual strains along the outer and the inner surfaces of both Sections S1-R and S3-R. Only small differences are found between these two predicted distributions due to i) different inner radii, and ii) different numbers of welding passes. Similar differences are also found between the predicted longitudinal residual strains along the outer and the inner surfaces of both Sections S1-S and S3-S, as shown in Fig. 23.

3.3 Three-dimensional plots of residual stress distributions

After a thorough calibration of the proposed models against measured data, three-dimensional plots of the longitudinal residual stresses of both Sections S3-R and S3-S are illustrated in Fig. 24. These plots present a clear illustration on the residual stress distributions in the CFSHS induced by transverse bending and longitudinal welding as follows:

a) Residual stresses at the round corners

These residual stresses have a large variation across the plate thickness of the round corners, i.e. from tensile stresses at the outer surface to compressive stresses at the inner surface. The stress patterns remain constant throughout the round corners. It should be noted that the magnitudes of these stresses are directly related to the inner radius to plate thickness ratios R_{in} / t of the sections.

b) Residual stresses in the vicinity of the welding seams

Large residual tensile stresses are induced in the vicinity of the welding seams of the sections, and these stresses are highly uniform across the plate thicknesses. It should be noted that complementary residual compressive stresses are induced in the rest of the sections, and the values of these compressive stresses are very small, when compared with those large tensile stresses which act over only small areas in the sections. Hence, force equilibrium due to welding-induced residual stresses within the sections is achieved.

It is apparent that the residual stresses induced by longitudinal welding are larger than those induced by transverse bending with a factor of 2 to 3. It is agreed that those residual stresses induced by transverse bending do not affect those caused by longitudinal welding because these

stresses do not coincide within the cross-sections of these cold-formed square hollow sections. More importantly, both residual stresses should be accurately predicted and incorporated subsequently into the structural models of the cold-formed square hollow sections for determination of their structural behaviour as these residual stresses will affect both yielding and softening of the sections significantly.

3.3.1 Simplified residual stress patterns

In order to establish residual stress patterns of these sections for advanced structural analyses and design, it is proposed to simplify the residual stress distributions across the plate thicknesses in the models. Fig. 25 illustrates the distributions of the average residual stresses of Models S3-R and S3-S, and these stresses are considered as the full stress distributions.

These distributions are readily simplified with the use of step functions to describe the presence of significant residual stresses in both the round corners and the welding seams of the sections after consideration of force equilibrium in the sections. These simplified residual stress patterns with various parameters are also plotted in Fig. 25 for direct comparisons. Table 9 summarizes the values of these parameters for Sections S1-R to S4-R and S1-S to S4-S respectively.

4 Conclusions

In general, residual stresses are induced in structural members during various fabrication processes, such as welding, bending, press-braking, folding, flame cutting and punching. The presence of those residual stresses in cold-formed square hollow sections (CFSHS) primarily caused by i) transverse bending (or cold-forming), and ii) longitudinal welding, is widely

considered to have modified both initial stress and strain conditions of these steel members significantly. Hence, these residual stresses are widely considered to have significant adverse effects onto the structural performance of these CFSHS under various actions.

In order to examine and quantify both magnitudes and distributions of these residual stresses in S690 CFSHS, an investigation is undertaken to measure residual stresses due to transverse bending and longitudinal welding. Moreover, an approach of integrated numerical simulations is adopted in which a total of three co-ordinated finite element models are established together with various element types and block data transfers to generate compatible meshes for the following three analyses: i) two-dimensional (2-D) plane-strain bending analyses with large plastic deformations and springback, ii) three-dimensional (3-D) heat transfer analyses for transient temperature distributions under a heat source, and iii) three-dimensional (3-D) thermomechanical analyses for welding-induced residual stresses.

The predicted results of these three analyses have been carefully calibrated against various experimental data obtained from systematic measurements, such as surface temperatures during welding, and residual strains after welding. The key findings of this investigation are:

a) Through the proposed approach of an integrated numerical simulation using three co-ordinated finite element models, residual stresses in the S690 CFSHS induced by transverse bending and longitudinal welding have been successfully predicted after calibration against test data.

b) Typical three-dimensional plots of the complete residual stress distributions within typical S690 CFSHS are illustrated to present a clear picture of their initial stress conditions. Simplified residual stress patterns of these sections with specific values and parameters are also provided for subsequent advanced structural analyses and design.

c) The proposed modelling technique for transverse bending and longitudinal welding with compatible meshes of two-dimensional and three-dimensional models with various element types and block data transfers is demonstrated to be highly effective. The technique is readily applicable to simulate residual stresses of all fabricated sections manufactured with transverse bending and longitudinal welding, and, thus, the simulated residual stresses can be incorporated in subsequent structural analyses of all fabricated members.

Acknowledgments

The research project leading to publication of this paper is funded by the Research Grants Council of the University Grants Committee of the Government of Hong Kong (Project Nos. 152194/15E, 152687/16E and 152231/17E). Both technical and financial support from the Chinese National Engineering Research Centre for Steel Construction (Hong Kong Branch) funded by the Innovation and Technology Commission of the Government of Hong Kong SAR (Project No.: CNERC-Steel/BBY3), and the Research Committee of the Hong Kong Polytechnic University (Project No.: BBY6) is gratefully acknowledged. The research work reported in this paper is part of the research studies of the first, the second and the third authors who are supported by the Research Committee of The Hong Kong Polytechnic University (Project Nos.: RUQV, RTZX and RJLY). Supply of the high strength S690 steel by the Nanjing

Iron and Steel Co. Ltd. in Nanjing and fabrication of the cold-formed square hollow sections by Pristine Steel Engineering Co. Ltd. in Dongguan are gratefully acknowledged.

References

[1] ASTM. (2018). ASTM A514/A514M-18e1: Standard specification for high-yield-strength, quenched and tempered alloy steel plate, suitable for welding. ASTM International, West Conshohocken, PA, USA.

[2] CEN. (2019a). Hot rolled products of structural steels - Part 6: Technical delivery conditions for flat products of high yield strength structural steels in the quenched and tempered condition. BS EN 10025-6:2019, European Committee for Standardization (CEN), Brussels, Belgium.

[3] CNS. (2018). GB/T 1591-2018: High strength low alloy structural steel. China Standards Press, Beijing, China.

[4] Ma, T.Y., Liu, X., Hu, Y.F., Chung, K.F. & Li, G.Q. (2018). Structural behaviour of slender columns of high strength S690 steel welded H-sections under compression. Engineering Structures, 157: 75-85.

[5] Liu, X., & Chung, K. F. (2018). Experimental and numerical investigation into temperature history and residual stress distributions of high strength steel S690 welded H-sections. Engineering Structures, 165, 396-411.

[6] Liu, X., Chung, K. F., Huang, M., Wang, G., & Nethercot, D. A. (2019). Thermomechanical parametric studies on residual stresses in S355 and S690 welded H-sections. Journal of Constructional Steel Research, 160, 387-401.

[7] Withers, P. J., & Bhadeshia, H. K. D. H. (2001). Residual stress. Part 1 – Measurement techniques. Materials Science and Technology, 17(4), 355-365.

[8] Rossini, N. S., Dassisti, M., Benyounis, K. Y., & Olabi, A. G. (2012). Methods of measuring residual stresses in components. Materials & Design, 35, 572-588.

[9] Ban, H., Shi, G., Shi, Y., & Wang, Y. (2012). Residual stress tests of high-strength steel equal angles. Journal of Structural Engineering, 138(12), 1446-1454.

[10] Wang, Y. B., Li, G. Q., & Chen, S. W. (2012). The assessment of residual stresses in welded high strength steel box sections. Journal of Constructional Steel Research, 76, 93-99.

[11] Ban, H., Shi, G., Shi, Y., & Wang, Y. (2013a). Residual stress of 460 MPa high strength steel welded box section: Experimental investigation and modeling. Thin-Walled Structures, 64, 73-82.

[12] Ban, H., Shi, G., Bai, Y., Shi, Y., & Wang, Y. (2013b). Residual stress of 460 MPa high strength steel welded I section: experimental investigation and modeling. International Journal of Steel Structures, 13(4), 691-705.

[13] Li, T. J., Li, G. Q., & Wang, Y. B. (2015). Residual stress tests of welded Q690 high-strength steel box-and H-sections. Journal of Constructional Steel Research, 115, 283-289.

[14] Ma, J. L., Chan, T. M., & Young, B. (2015). Material properties and residual stresses of cold-formed high strength steel hollow sections. Journal of Constructional Steel Research, 109, 152-165.

[15] Yang, C., Yang, J., Su, M., & Li, Y. (2017). Residual stress in high-strength-steel welded circular tubes. Proceedings of the Institution of Civil Engineers - Structures and Buildings, 170(9), 631-640.

[16] Somodi, B., & Kövesdi, B. (2017). Residual stress measurements on cold-formed HSS hollow section columns. Journal of Constructional Steel Research, 128, 706-720.

[17] Somodi, B., & Kövesdi, B. (2018). Residual stress measurements on welded square box sections using steel grades of S235–S960. Thin-Walled Structures, 123, 142-154.

[18] Chen, J., & Chan, T. M. (2020). Material properties and residual stresses of cold-formed high-strength-steel circular hollow sections. Journal of Constructional Steel Research, 170, 106099.

[19] Hu, Y. F., Chung, K. F., Ban, H., & Nethercot, D. A. (2020). Investigations into residual stresses in S690 cold-formed circular hollow sections due to transverse bending and longitudinal welding. Engineering Structures, 219, 110911.

[20] Lee, C. K., Chiew, S. P., & Jiang, J. (2012a). Residual stress study of welded high strength steel thin-walled plate-to-plate joints. Part 1: Experimental study. Thin-Walled Structures, 56, 103-112.

[21] Lee, C. K., Chiew, S. P., & Jiang, J. (2014a). Residual stress of high strength steel box T-joints: Part 1: Experimental study. Journal of Constructional Steel Research, 93, 20-31.

[22] Khan, M., Paradowska, A., Uy, B., Mashiri, F., & Tao, Z. (2016). Residual stresses in high strength steel welded box sections. Journal of Constructional Steel Research, 116, 55-64.

[23] Goldak, J., Chakravarti, A., & Bibby, M. (1984). A new finite element model for welding heat sources. Metallurgical transactions B, 15(2), 299-305.

[24] Nguyen, N. T., Ohta, A., Matsuoka, K., Suzuki, N., & Maeda, Y. (1999). Analytical solutions for transient temperature of semi-infinite body subjected to 3-D moving heat sources. Welding Journal, 78, 265-s.

[25] Fachinotti, V. D., Anca, A. A., & Cardona, A. (2011). Analytical solutions of the thermal field induced by moving double- ellipsoidal and double- elliptical heat sources in a semi- infinite body. International Journal for Numerical Methods in Biomedical Engineering, 27(4), 595-607.

[26] Lee, C. K., Chiew, S. P., & Jiang, J. (2012b). Residual stress study of welded high strength steel thin-walled plate-to-plate joints. Part 2: Numerical modeling. Thin-walled structures, 59, 120-131.

[27] Lee, C. K., Chiew, S. P., & Jiang, J. (2014b). Residual stress of high strength steel box T-joints Part 2: Numerical study. Journal of Constructional Steel Research, 98, 73-87.

[28] Jiang, J., Chiew, S. P., Lee, C. K., & Tiong, P. L. Y. (2017). A numerical study on residual stress of high strength steel box column. Journal of Constructional Steel Research, 128, 440-450.

[29] Ni, J., Zhuang, X., & Abdel Wahab, M. (2020). Review on the prediction of residual stress in welded steel components. CMC-Computers Materials & Continua 62:2, 495-523.

[30] Alhafadhi, M. H., & Krallics, G. (2020). Numerically simulated prediction of residual stresses in welding considering phase transformation effects. In Journal of Physics: Conference Series 1527: 1, p. 012017. IOP Publishing.

[31] Zhang, K., Dong, W., & Lu, S. (2021). Finite element and experiment analysis of welding residual stress in S355J2 steel considering the bainite transformation. Journal of Manufacturing Processes 62: 80-89.

[32] Tankova, T., da Silva, L. S., Balakrishnam, M., Rodrigues, D., Launert, B., Pasternak, H., & Tun, T. Y. (2019). Residual stresses in welded I section steel members. Engineering Structures, 197: 109398.

[33] CEN. (2019b). Metallic materials - Tensile testing - Part 1: Method of test at room temperature. BS EN ISO 6892-1:2009, European Committee for Standardization (CEN), Brussels, Belgium.

[34] Abaqus 6.13. (2013). ABAQUS Analysis User's Manual, version 6.13.

[35] CEN. (2009). Eurocode 3 - Design of steel structures - Part 1-2: General rules - Structural fire design. BS EN 1993-1-2:2005, European Committee for Standardization (CEN), Brussels, Belgium.

[36] CEN. (2007). Eurocode 3 - Design of steel structures - Part 1-12: Additional rules for the extension of EN 1993 up to steel grades S 700. BS EN 1993-1-12:2007, European Committee for Standardization (CEN), Brussels, Belgium.

[37] Liu, X., Chung, K. F., Ho, H. C., Xiao, M., Hou Z. X., & Nethercot, D. A. (2018). Mechanical behavior of high strength S690-QT steel welded sections with various heat input energy. Engineering Structures 175:245-256,

[38] Ho, H. C., Chung, K. F., Huang, M. X., Nethercot, D. A., Liu, X., Jin, H., Wang, G. D. & Tian, Z. H. (2020). Mechanical properties of high strength S690 steel welded sections through tensile tests on heat-treated coupons. Journal of Constructional Steel Research, 166, 105922.

759

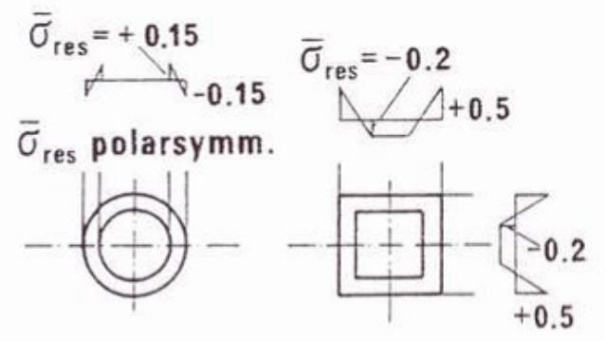

a) Rolled structural hollow sections

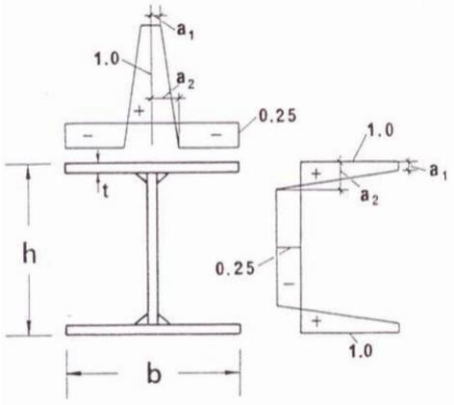

b) Welded H-sections

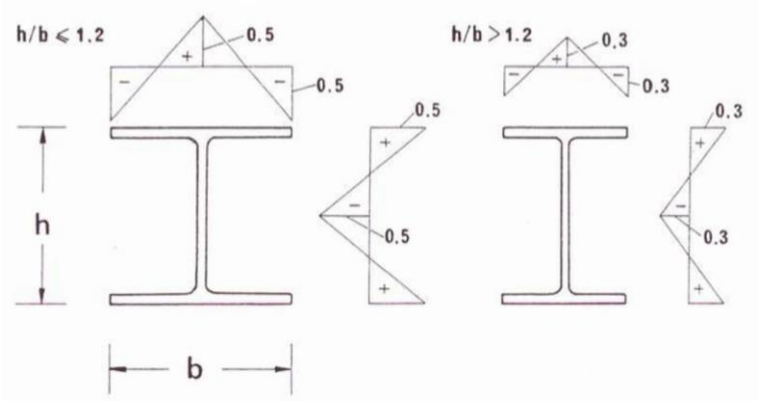

c) Rolled H-sections

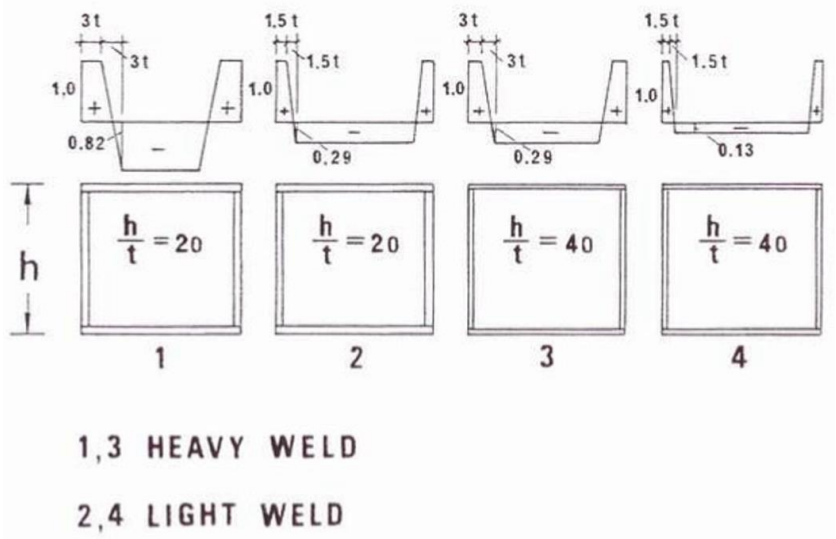

d) Welded box-sections

Fig. 1 Typical residual stress patterns due to welding (ECCS 1986)

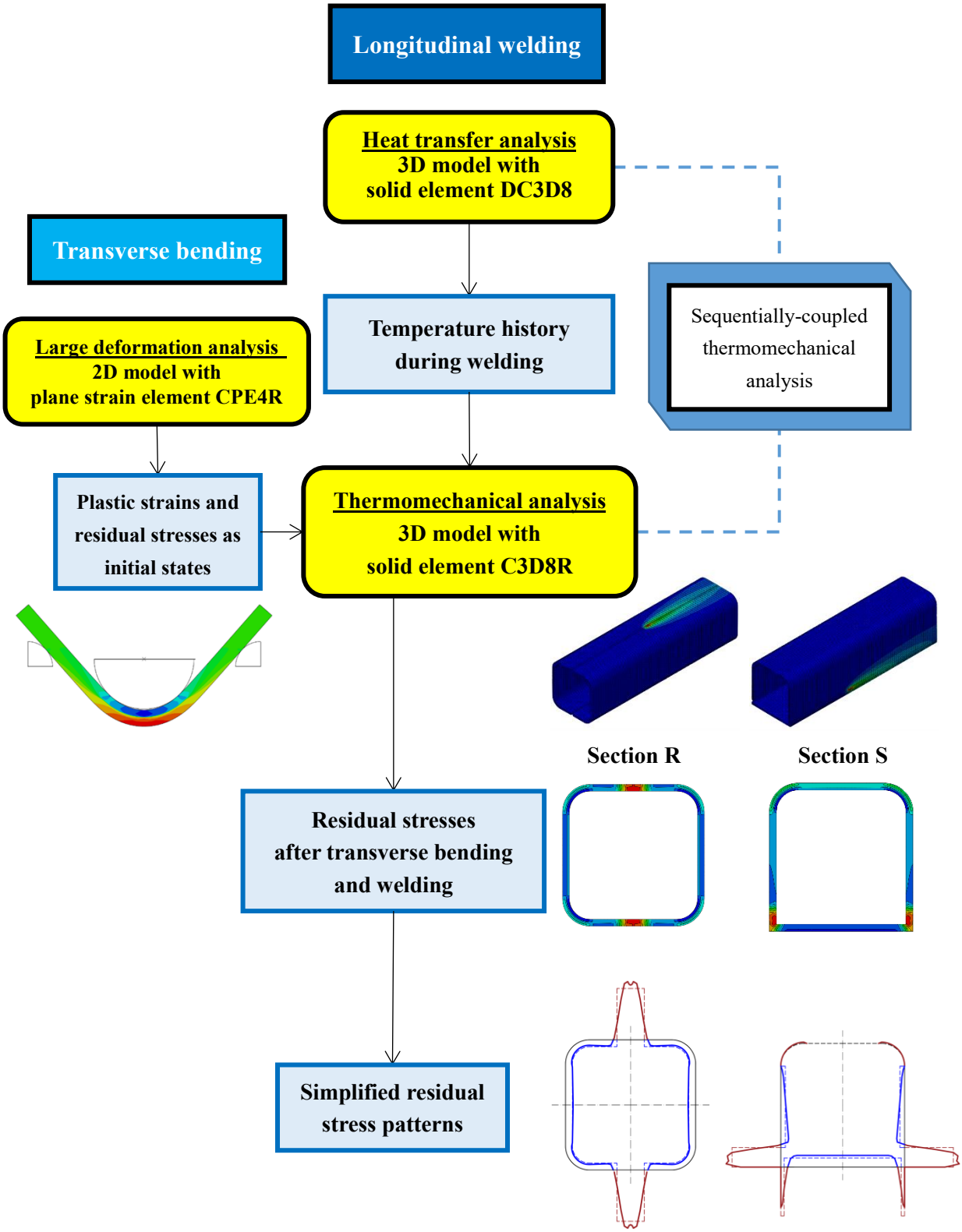

Fig. 2 Flowchart of an integrated numerical simulation for predicting residual stresses in CFSHS

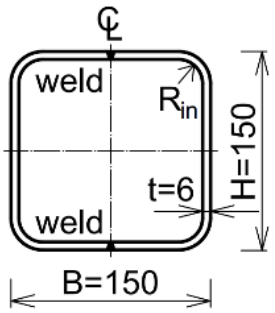

a) Section S1-R
150 x 150 x 6 CFSHS

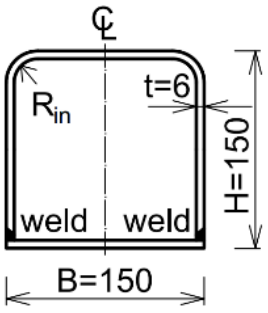

b) Section S1-S
150 x 150 x6 CFSHS

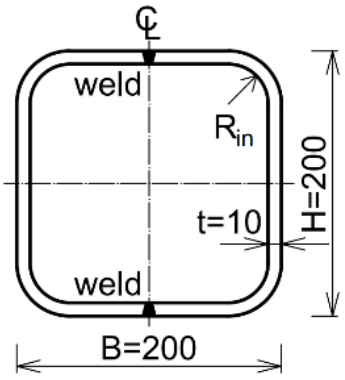

c) Section S3-R
200 x 200 x 10 CFSHS

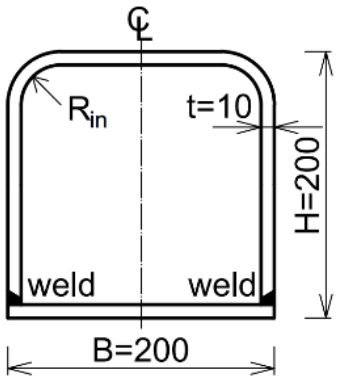

d) Section S3-S
200 x 200 x 10 CFSHS

Note: All dimensions are in mm.

Fig. 3 High strength S690 CFSHS under investigation

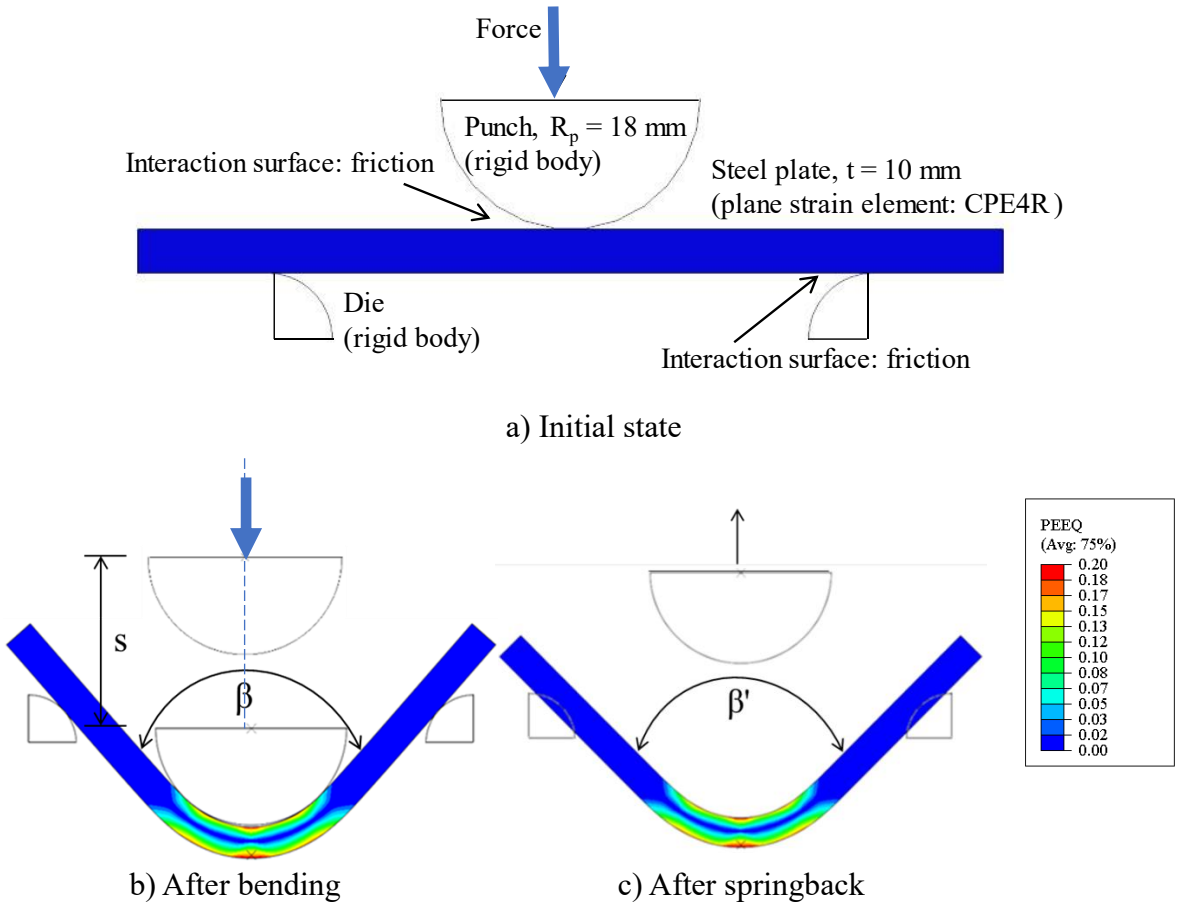

Fig. 4 Transverse bending simulated with 2D plane-strain model

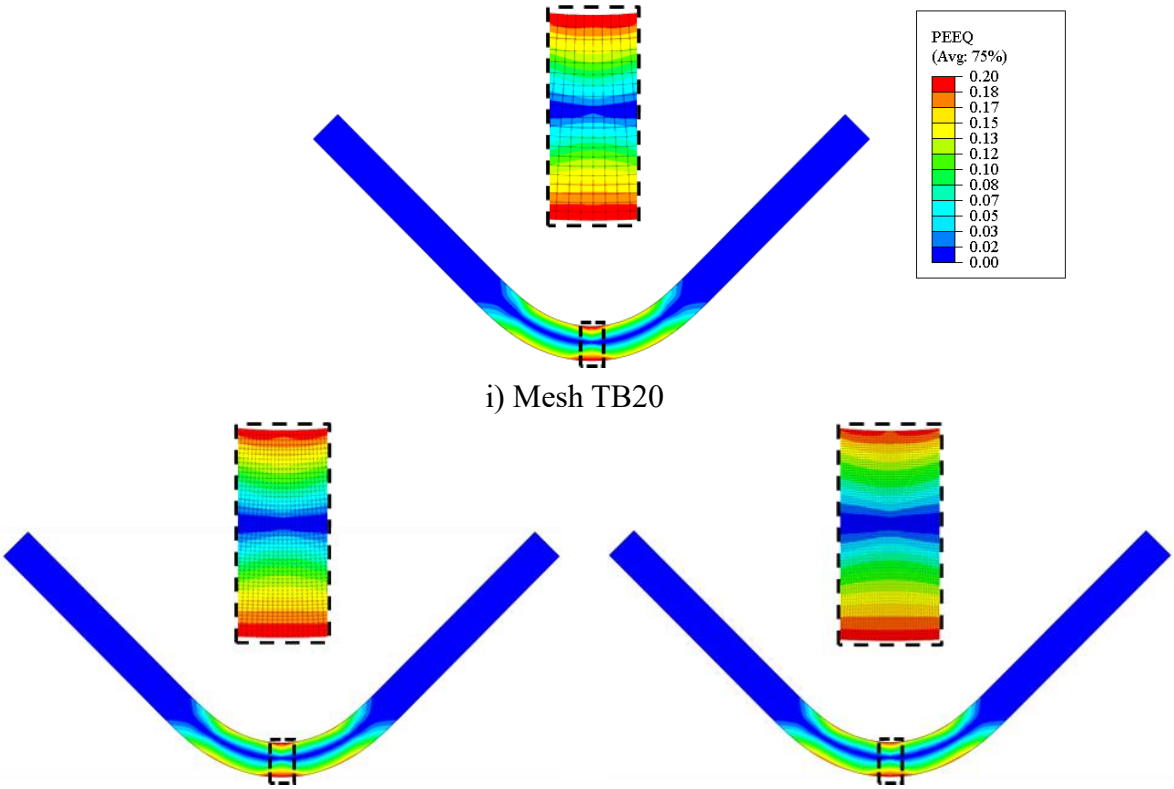

i) Mesh TB20

ii) Mesh TB50

iii) Mesh TB100

a) Equivalent plastic strains, PEEQ

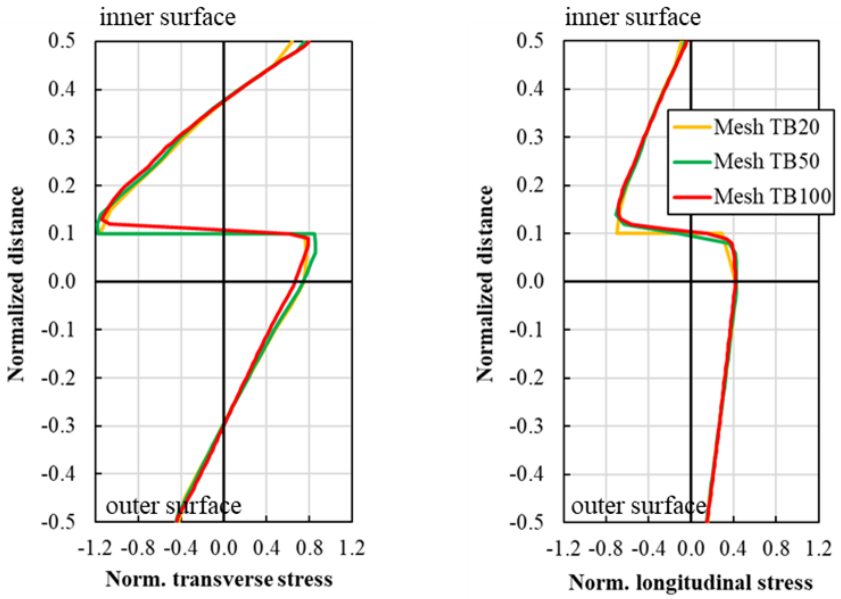

i) Transverse stresses, $\sigma_{res,t}$ ii) Longitudinal stresses, $\sigma_{res,l}$

b) Cross-sectional variations of residual stresses

Fig. 5 Residual strains and stresses along the centre lines of the cold-bent plates

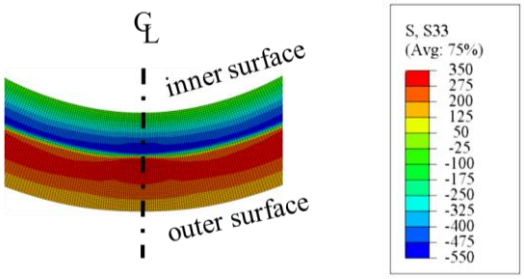

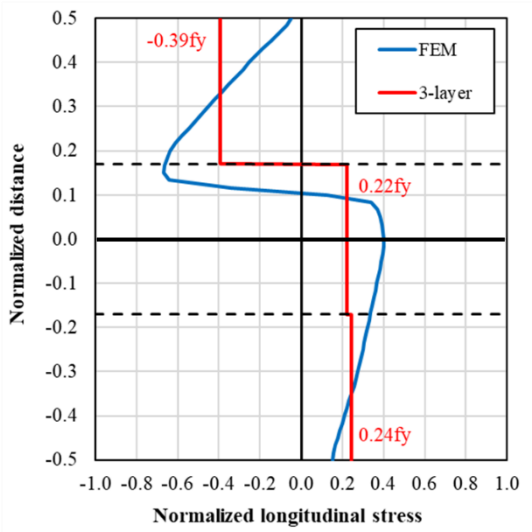

t = 6 mm, R_{in} = 18 mm

Mesh TB100

a) At the corner regions of 6 mm thick plates: Sections S1-R and S1-S

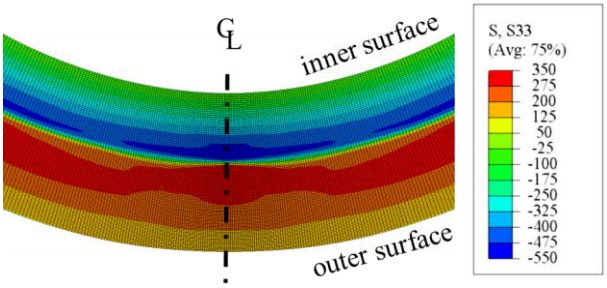

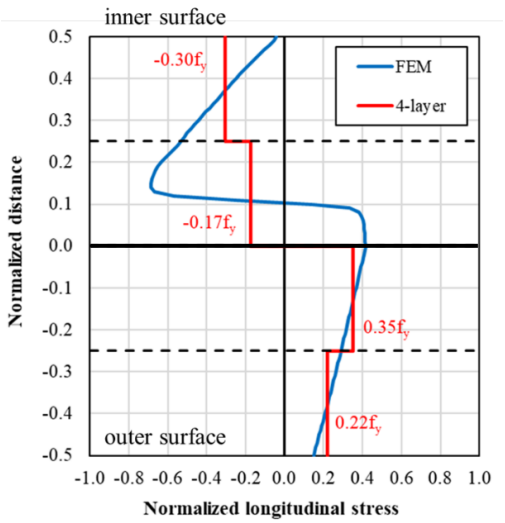

t = 10 mm, R_{in} = 30 mm

Mesh TB100

b) At the corner regions of 10 mm thick plates: Sections S3-R and S3-S

Fig. 6 Longitudinal residual stresses due to transverse bending

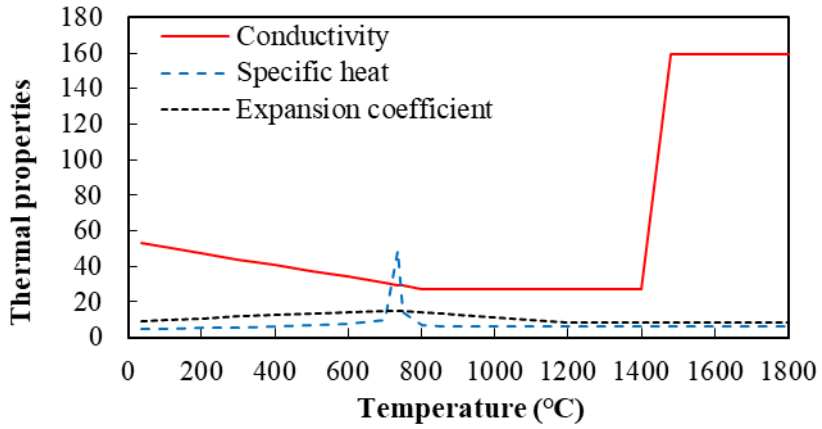

a) Thermal properties

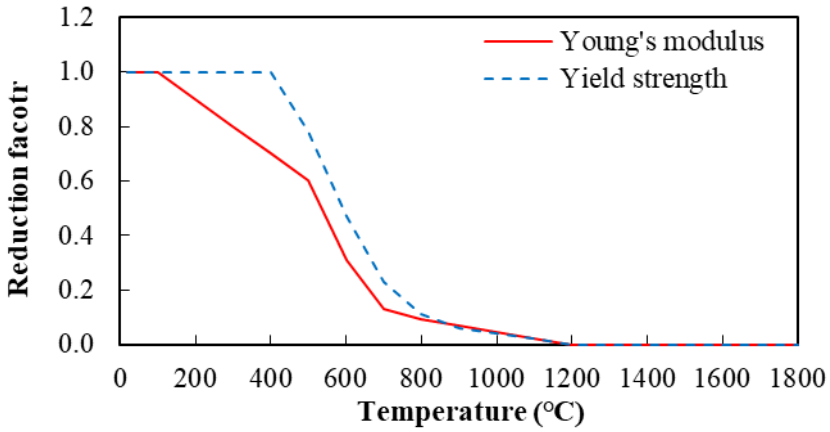

b) Reductions factors for Young's modulus and yield strength

Fig. 7 Reduced thermal and mechanical properties of S690 steels at elevated temperatures (CEN 2009)

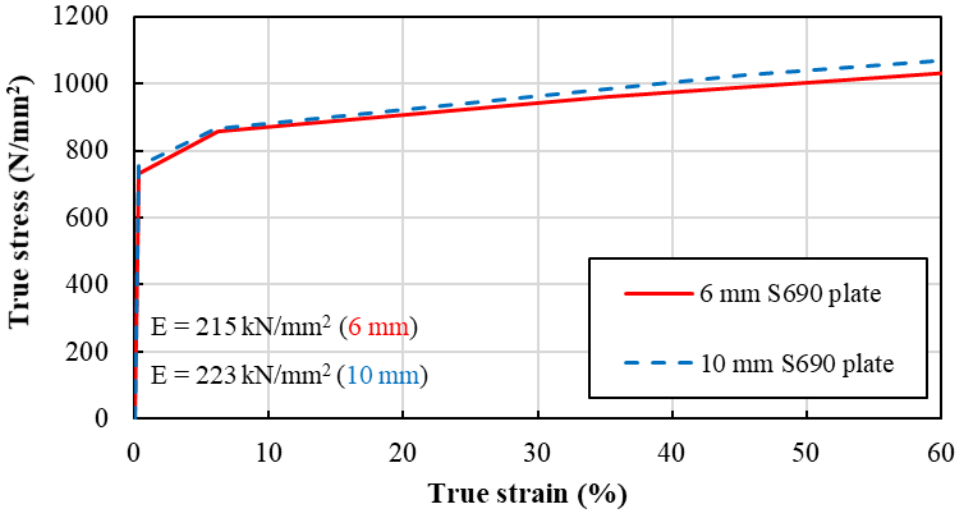

Fig. 8 True stress-strain curves at ambient temperatures

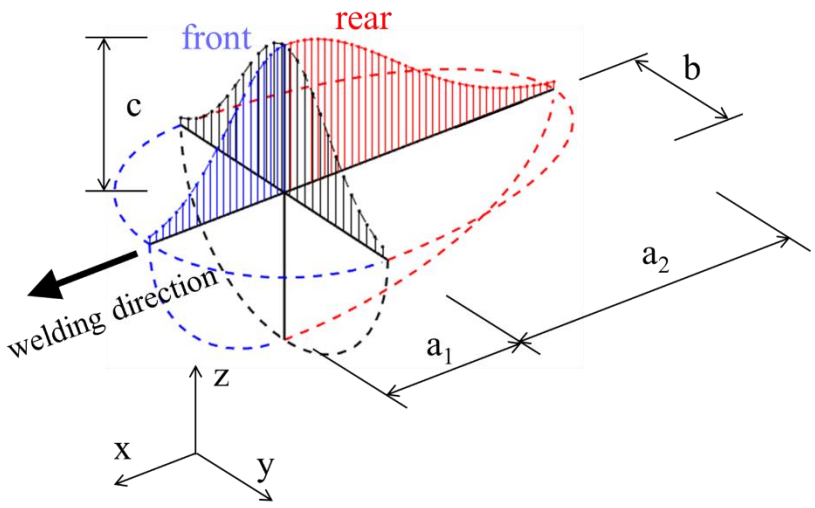

Fig. 9 Double-ellipsoidal heat source model (Goldak et al. 1984)

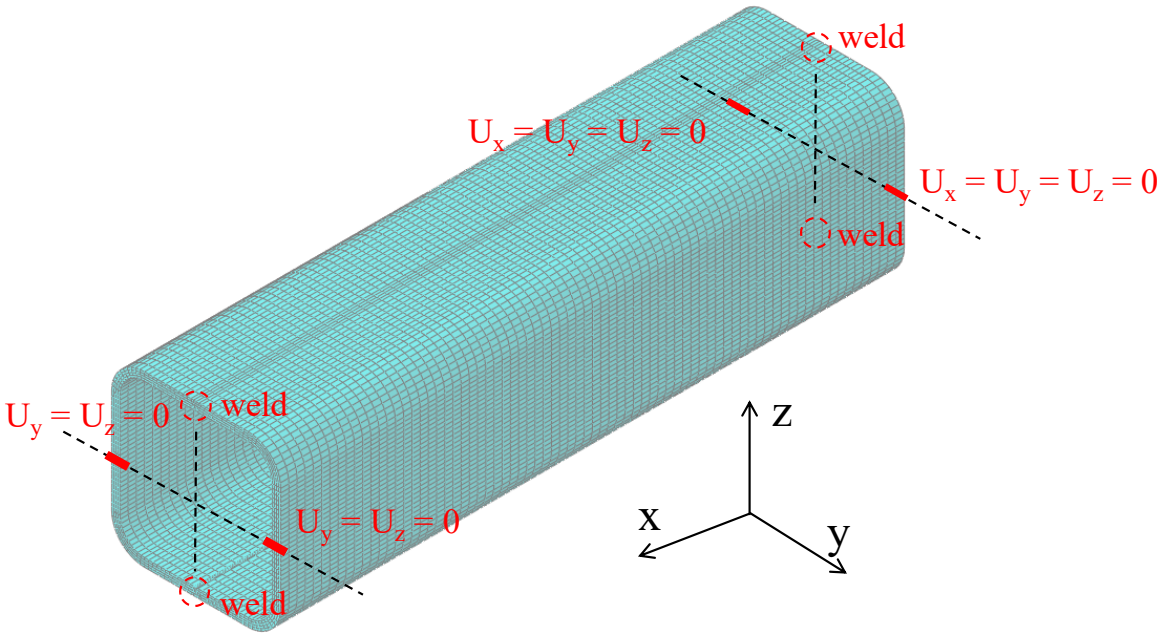

a) Section R

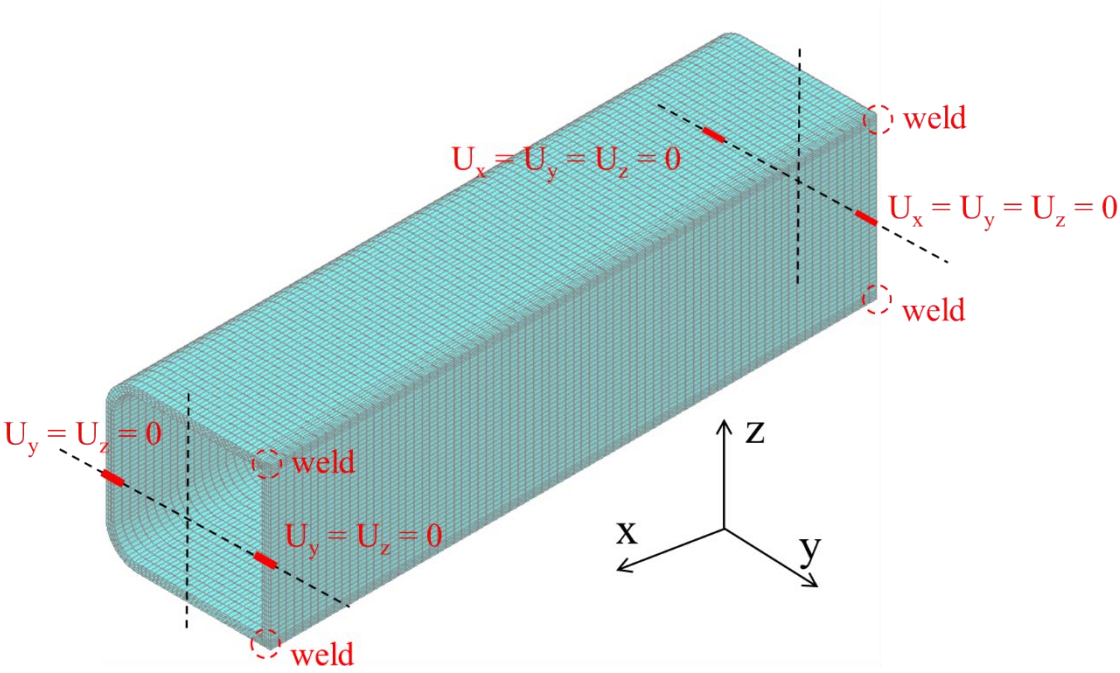

b) Section S

Fig. 10 Boundary conditions for both heat transfer and thermomechanical analyses

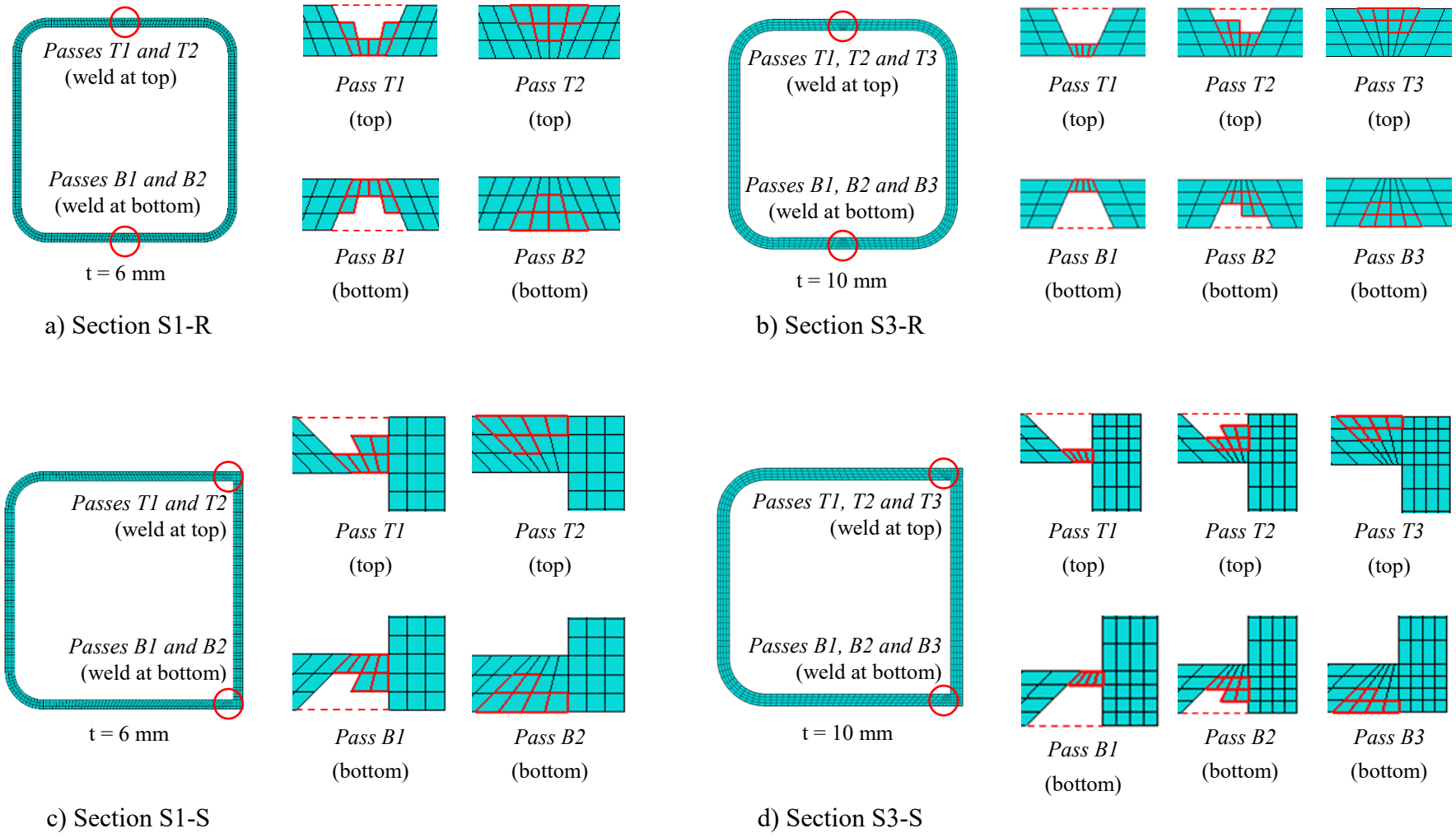

Fig. 11 Modelling of multi-pass welding in CFSHS

Section S3-R

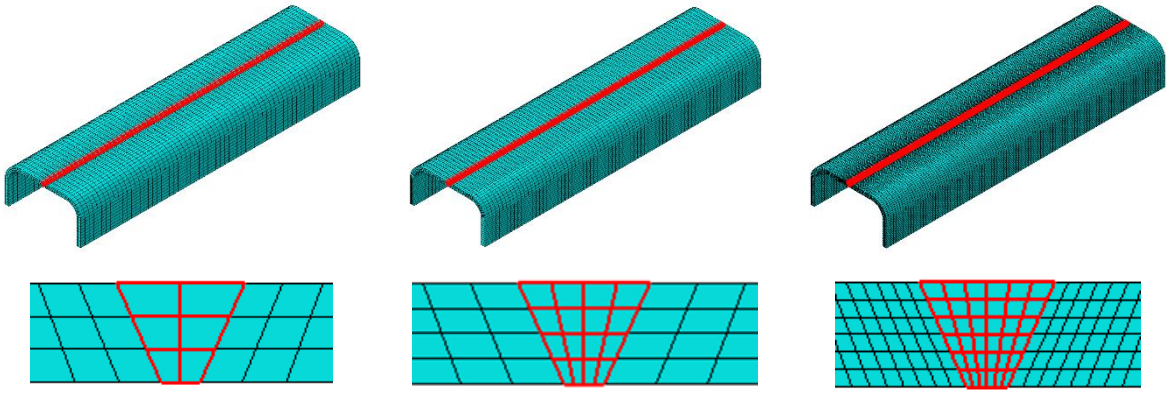

a) Mesh L03 b) Mesh L04 c) Mesh L06

Fig. 12 Mesh convergence study

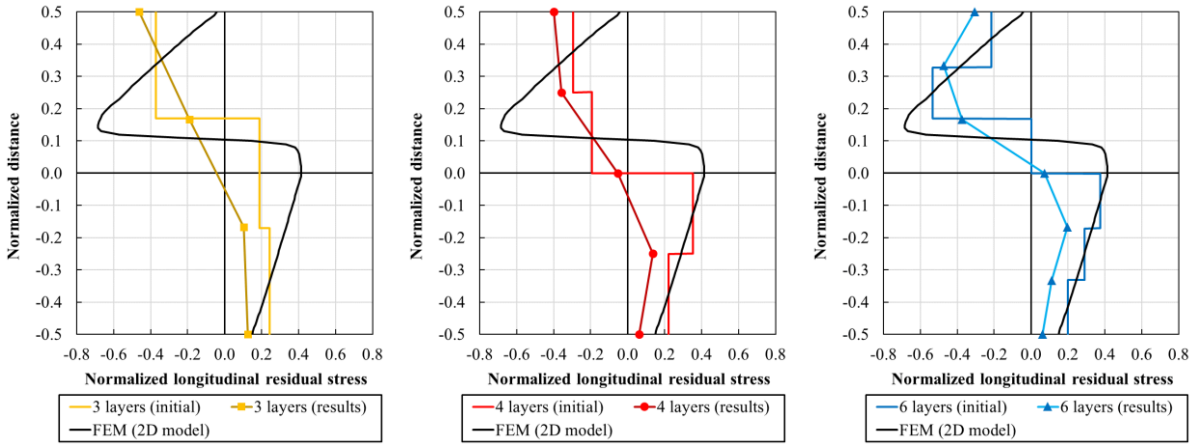

a) Mesh L03 b) Mesh L04 c) Mesh L06

Fig. 13 Longitudinal residual stresses due to transverse bending: initial states vs results

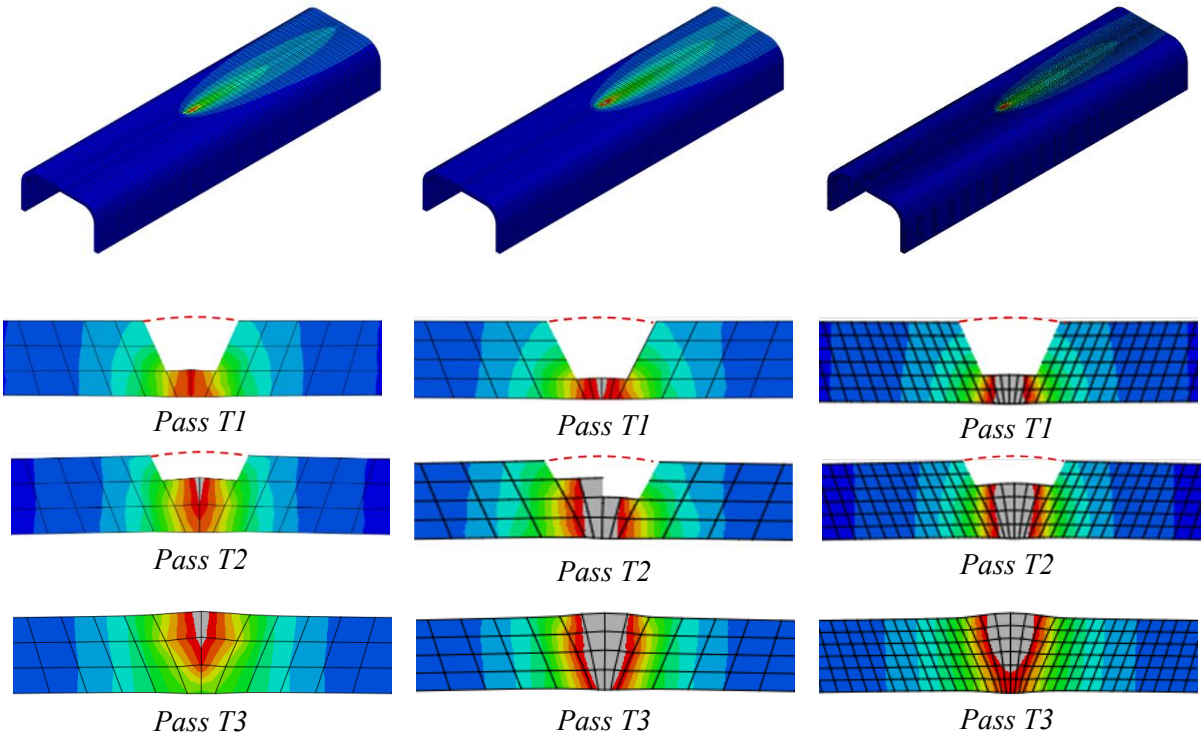

a) Mesh L03 b) Mesh L04 c) Mesh L06

Fig. 14 Temperature fields in heat transfer analyses

Note: Temperature range = 0 ~ 1400 ℃

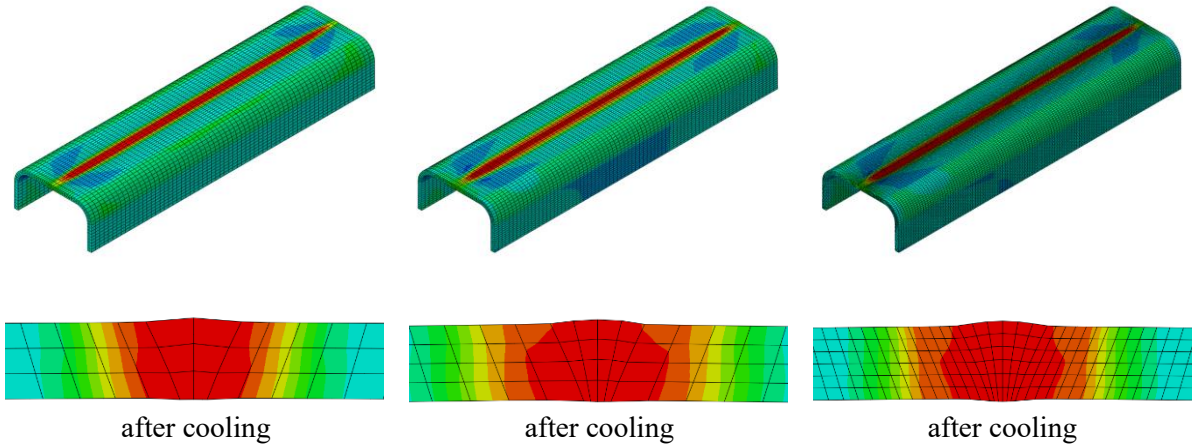

a) Mesh L03 b) Mesh L04 c) Mesh L06

Fig. 15 Longitudinal residual strains in thermomechanical analyses

Note: Strain range = -0.2 ~ 0.4 %

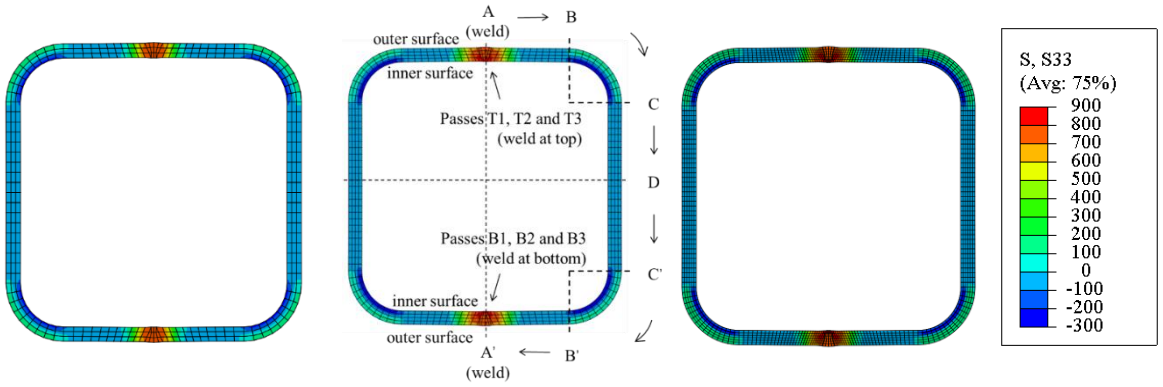

Mesh L03 Mesh L04 Mesh L06

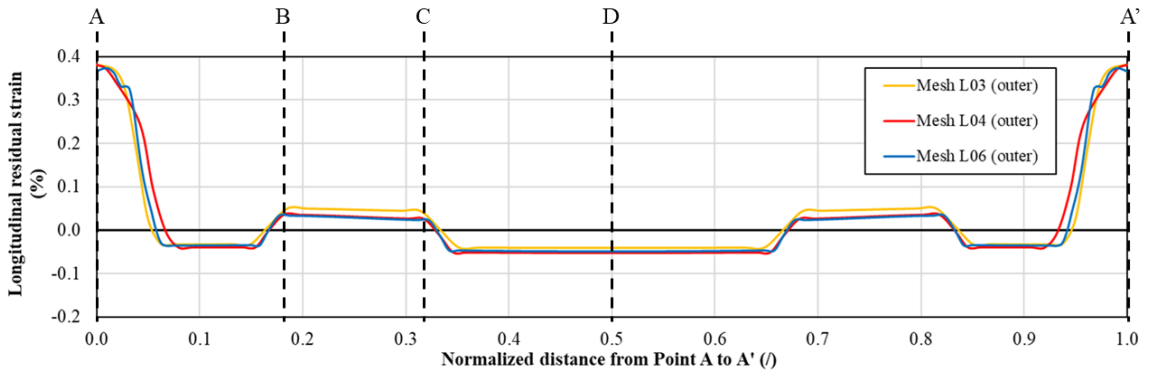

a) outer surface

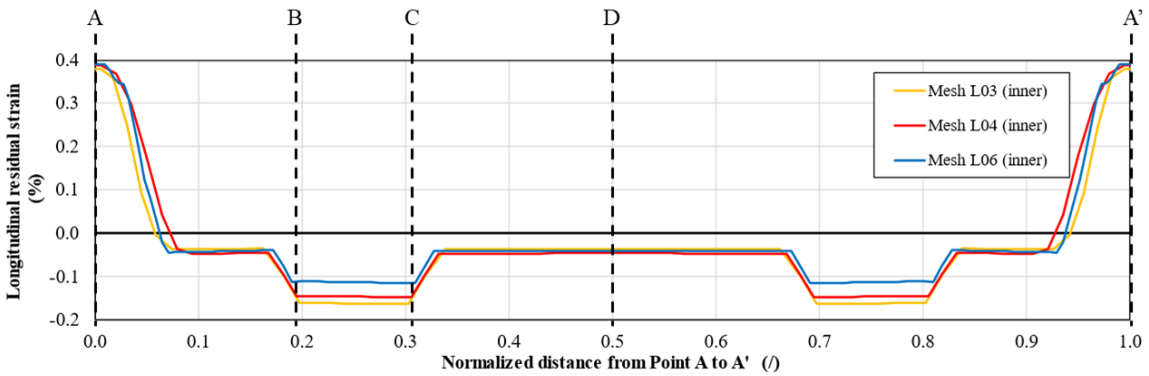

b) inner surface

Fig. 16 Longitudinal residual strains of mesh convergence study: Section S3-R

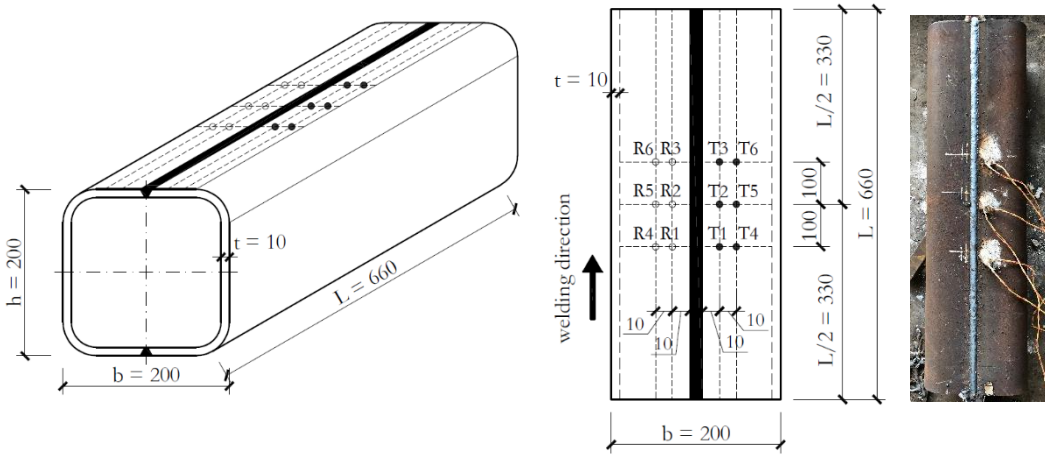

a) Section S3-R

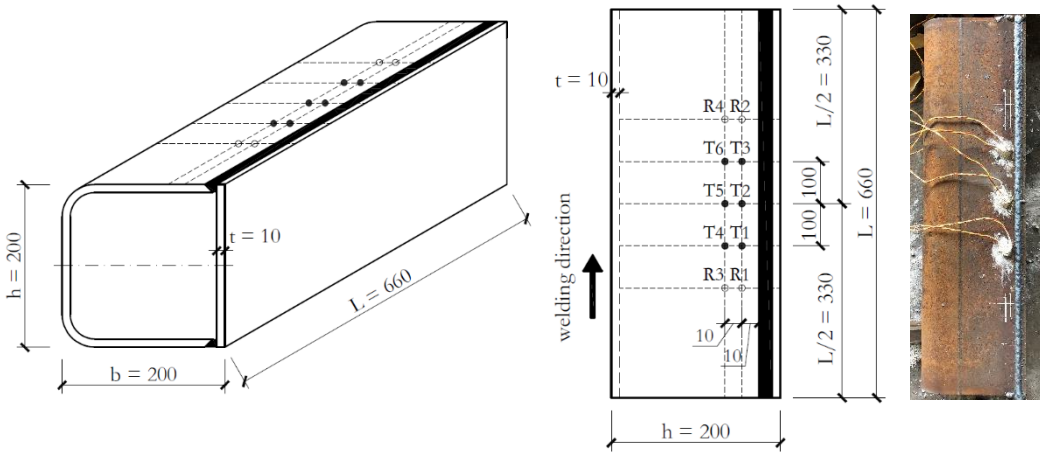

b) Section S3-S

Notes:

1. Points “R” denote the locations for temperature measurements with an infra-red camera.
2. All dimensions are in mm.

Fig. 17 Arrangements of instrumentation for temperature measurements

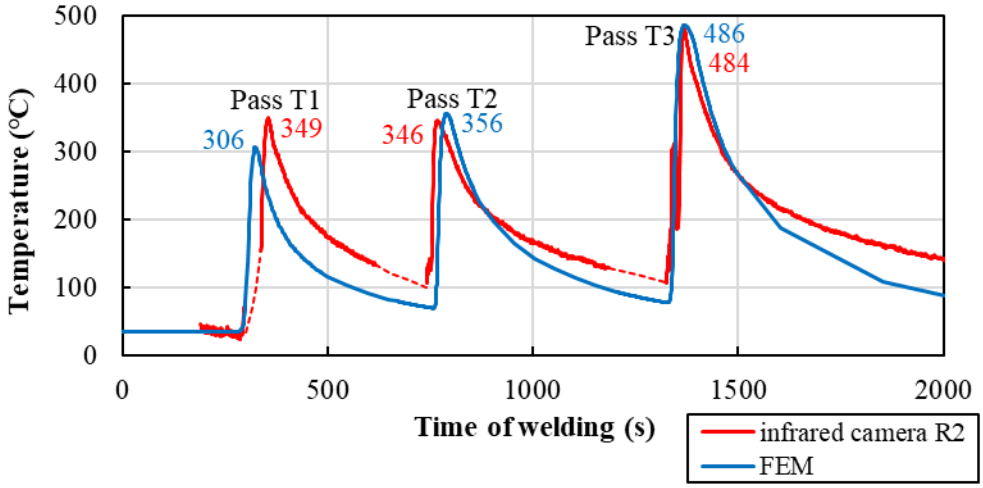

a) Section S3-R

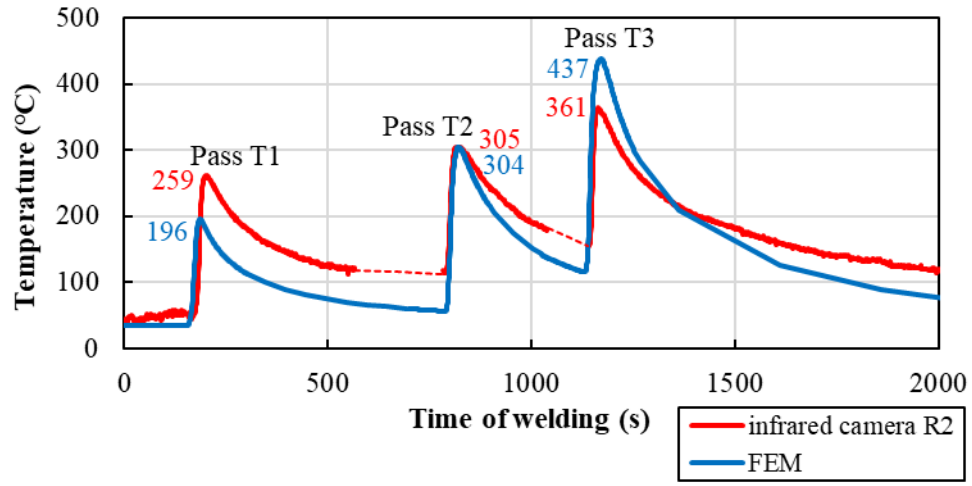

b) Section S3-S

Fig. 18 Temperature history at specific locations in Sections S3-R and S3-S

a) Section S3-R

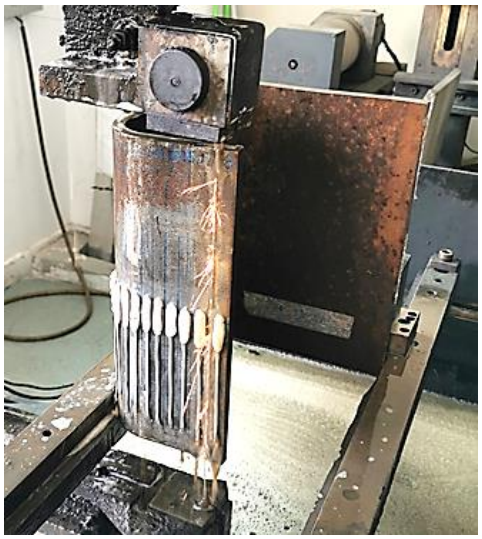

a) Wire cutting

c) Deformed strips cut from the Section

Fig. 19 Sectioning method

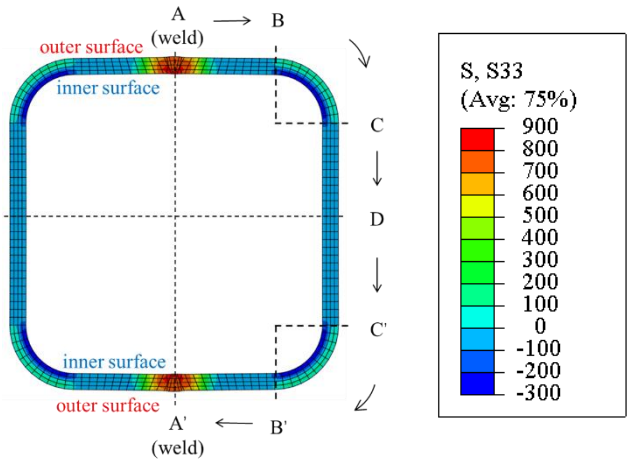

Section S3-R

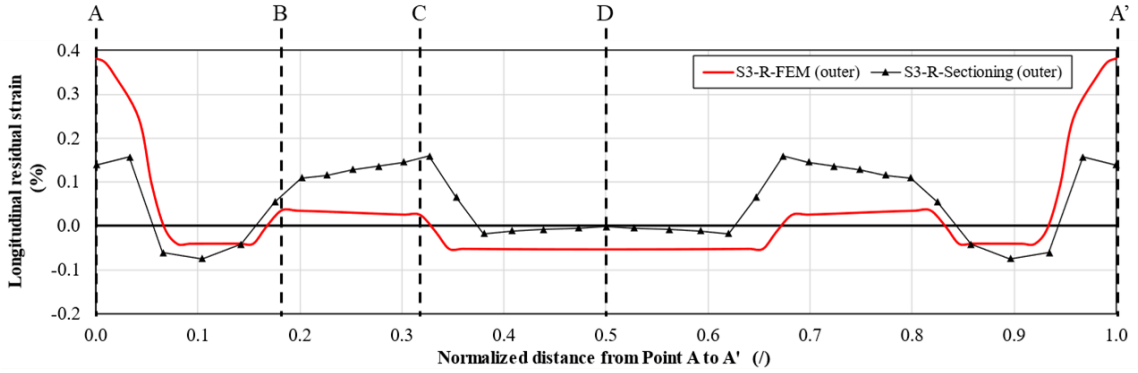

a) outer surface

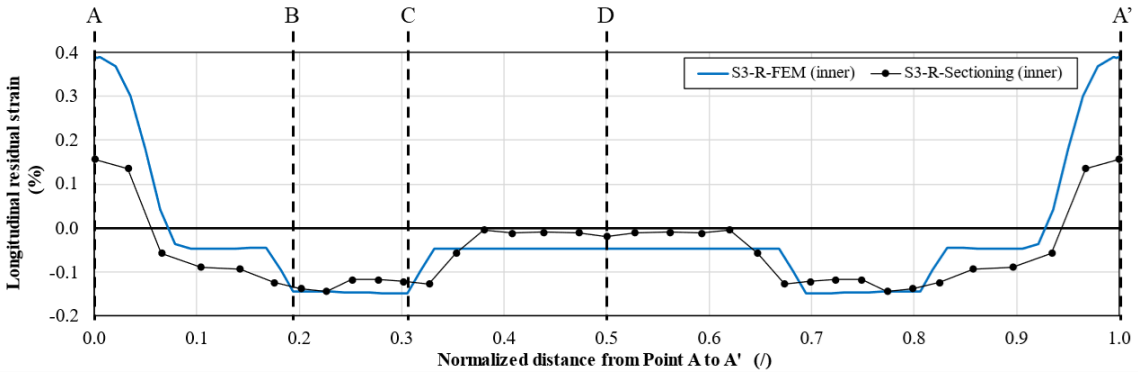

b) inner surface

Fig. 20 Longitudinal residual strains in Section S3-R: Predicted and measured data

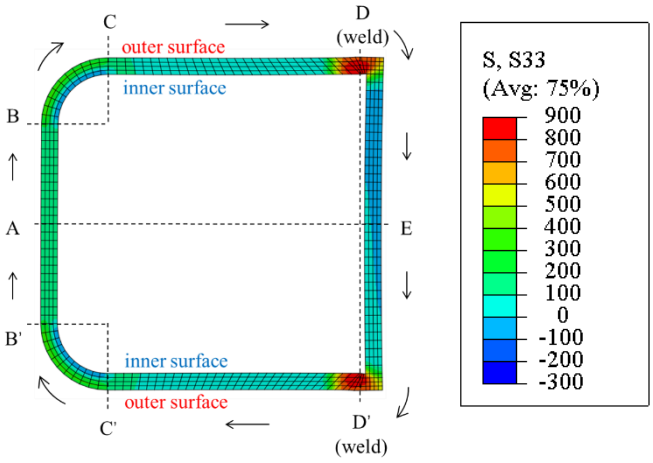

Section S3-S

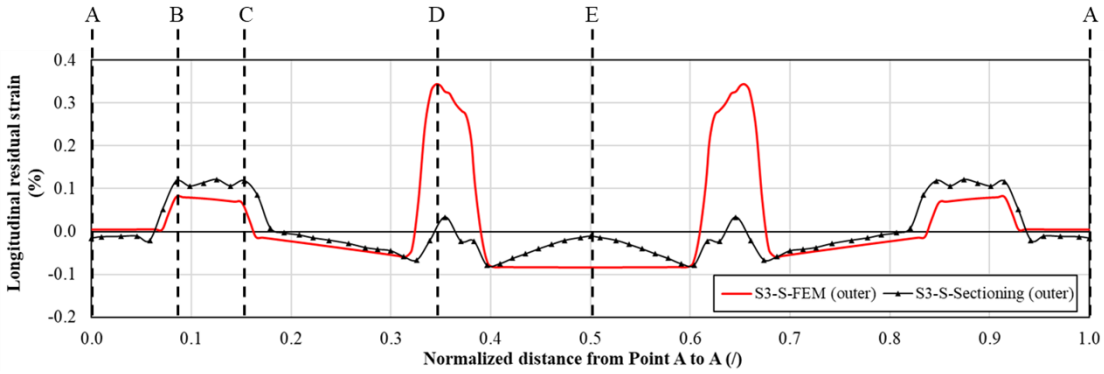

a) outer surface

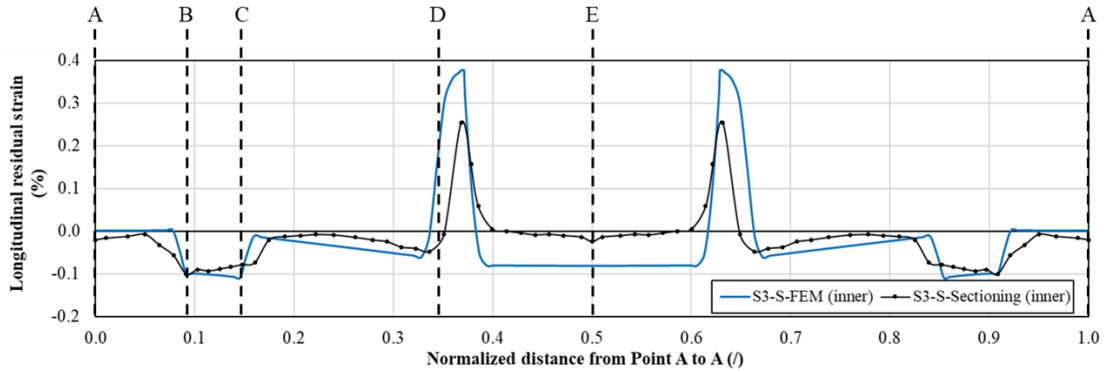

b) inner surface

Fig. 21 Longitudinal residual strains in Section S3-S: Predicted and measured data

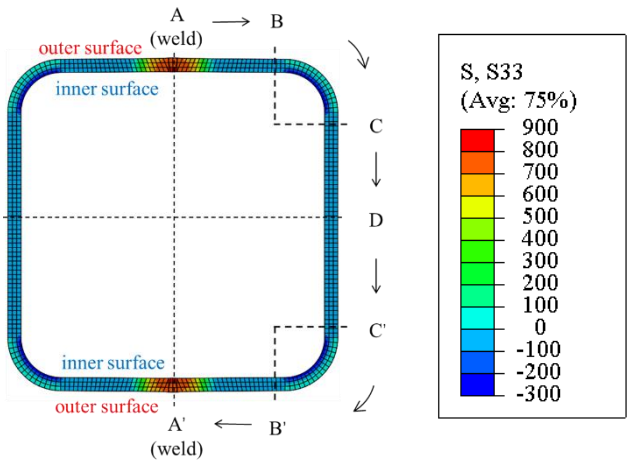

Section S1-R

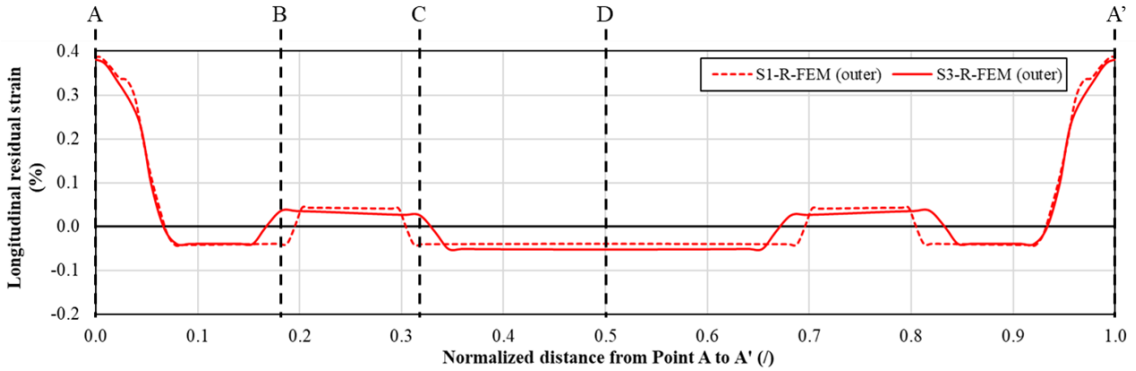

a) outer surface

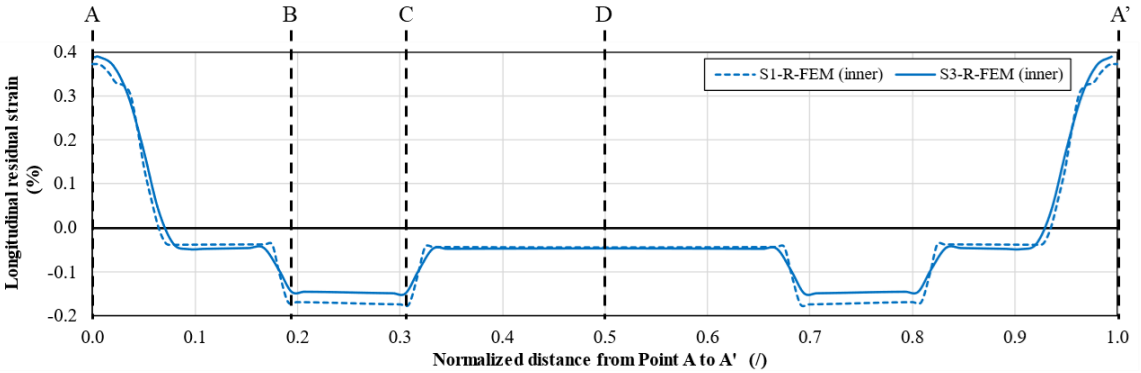

b) inner surface

Fig. 22 Longitudinal residual strains in Sections S1-R and S3-R

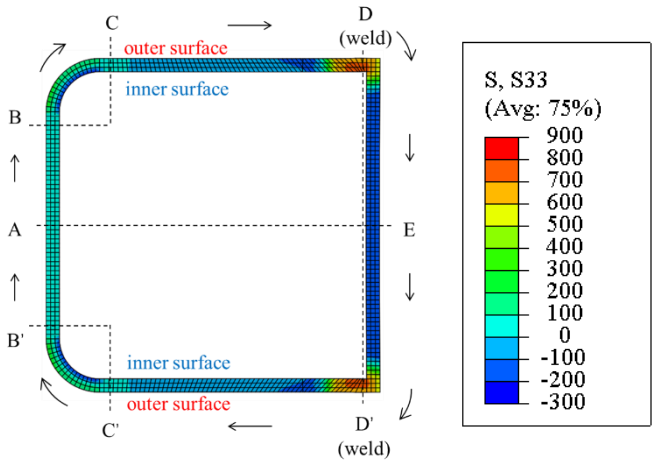

Section S1-S

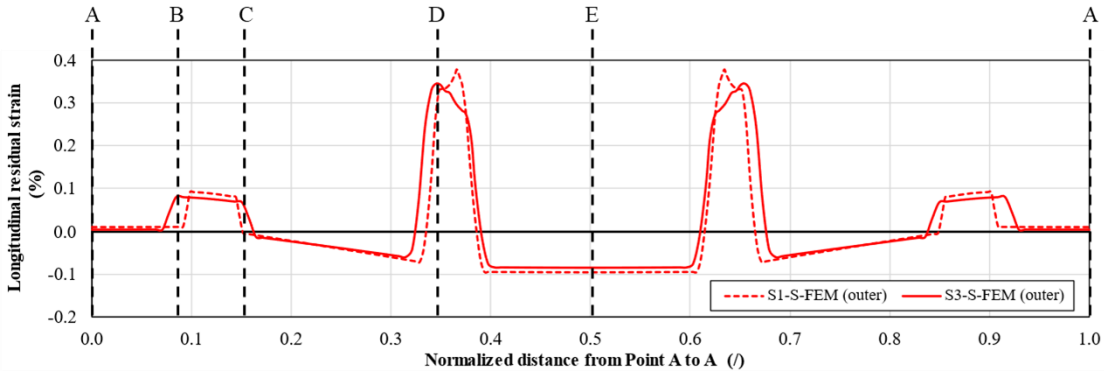

a) outer surface

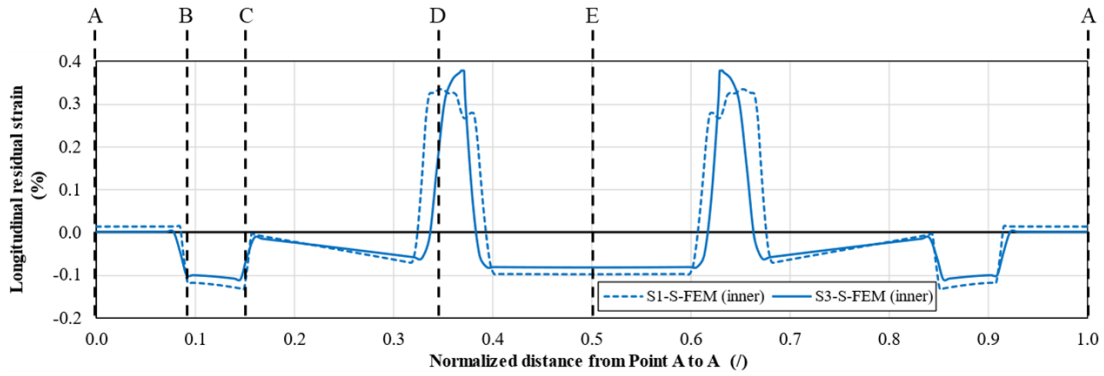

b) inner surface

Fig. 23 Longitudinal residual strains in Sections S1-S and S3-S

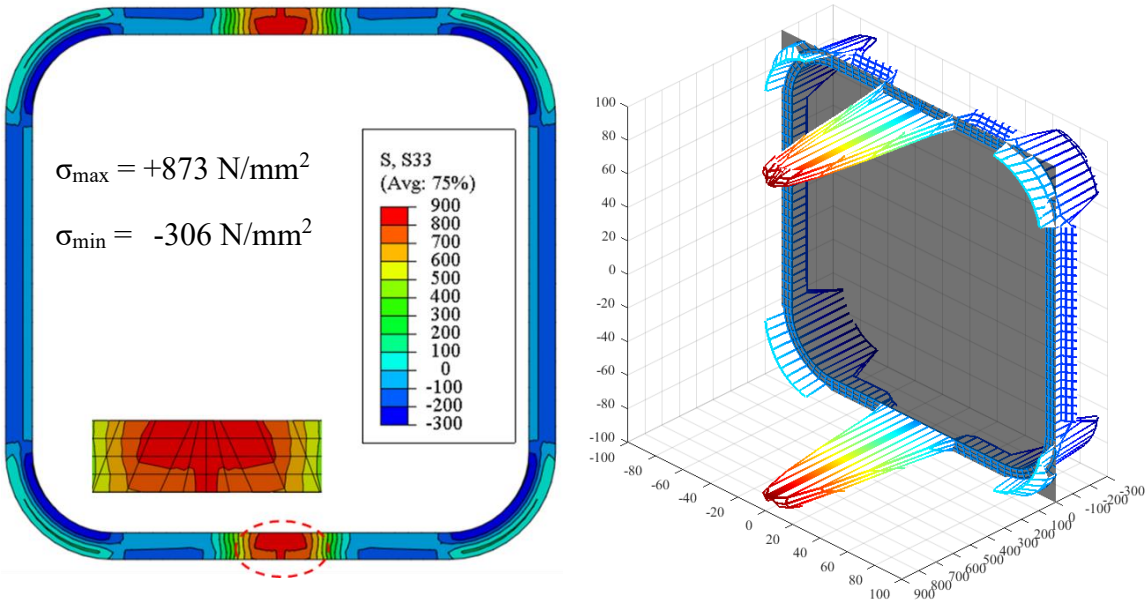

a) Section S3-R

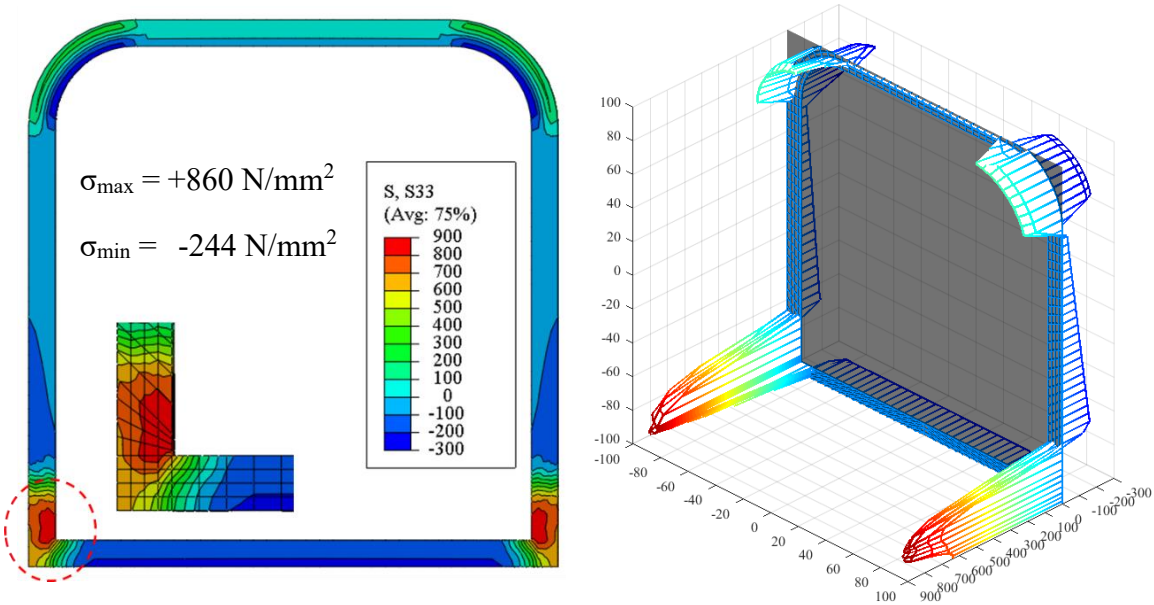

b) Section S3-S

Fig. 24 Three-dimensional plots of longitudinal residual stresses

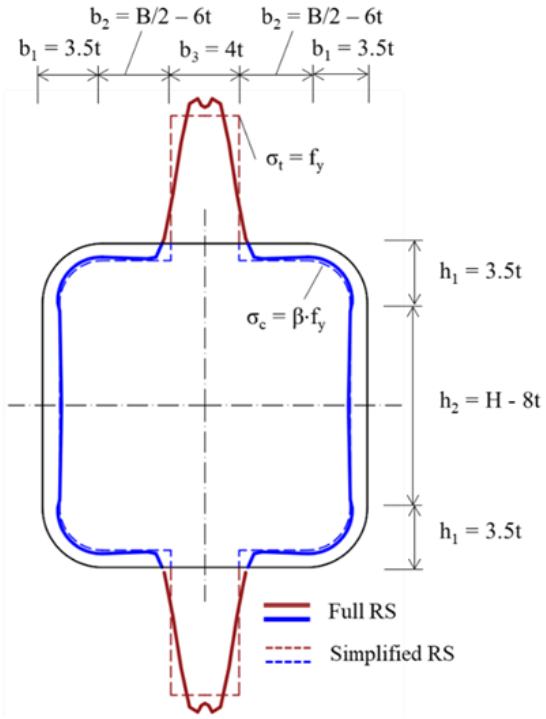

a) Section R

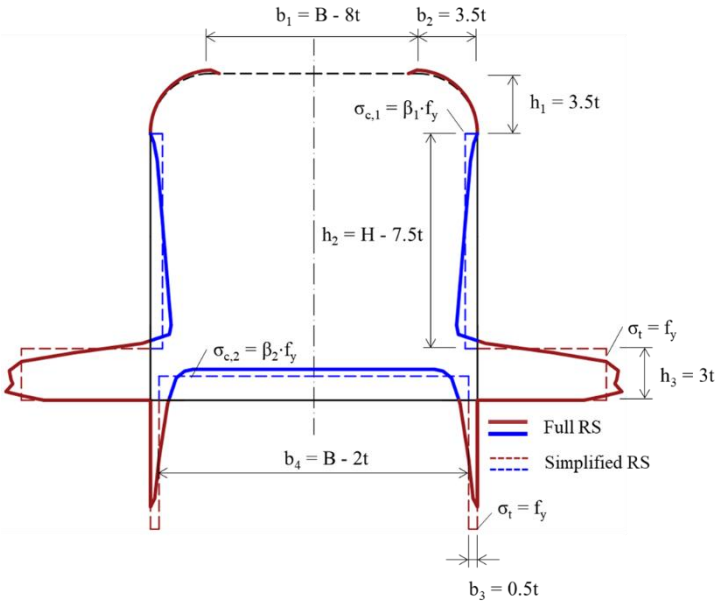

b) Section S

Fig. 25 Full distributions and simplified patterns of longitudinal residual stresses

Table 1 Recent studies on measurements of residual stresses in high strength steel welded sections

No.	References	Nominal yield strengths f_y (N/mm^2)	Type of welded sections	Measurement methods
1	Ban et al. (2012)	420	angles	sectioning
2	Lee et al. (2012a)	690	plate-to-plate joints	hole-drilling
3	Wang et al. (2012)	460	box sections	sectioning
4	Ban et al. (2013a)	460	box sections	sectioning
5	Ban et al. (2013b)	460	I-sections	sectioning
6	Lee et al. (2014a)	690	T-joints	hole-drilling
7	Li et al. (2015)	690	box and H-sections	sectioning
8	Ma et al. (2015)	460, 700 and 1100	CFCHS, CFRHS (roll-formed) and CFSHS (roll-formed)	sectioning
9	Khan et al. (2016)	690	box sections	neutron diffraction
10	Yang et al. (2017)	690	box sections	hole-drilling and sectioning
11	Somodi and Kövesdi (2017)	420 to 960	CFSHS (roll-formed)	sectioning
12	Somodi and Kövesdi (2018)	235 to 960	box sections	sectioning
13	Liu and Chung (2018)	690	H-sections	hole-drilling
14	Chen and Chan (2020)	460, 690 and 960	CFCHS	sectioning
15	Hu et al. (2020)	690	CFCHS	sectioning

Table 2 Investigation programme and scope of work

Section	Fabrication process		Experimental measurement			Numerical modelling		
	Transverse bending	Longitudinal welding	Welding parameters	Temperature history	Residual stresses	Transverse bending	Heat transfer analysis	Thermomechanical analysis
S1-R	Y	Y	Y	--	--	Y	Y	Y
S1-S	Y	Y	Y	--	--	Y	Y	Y
S3-R	Y	Y	Y	Y	Y	Y	Y	Y
S3-S	Y	Y	Y	Y	Y	Y	Y	Y

Table 3 Measured welding parameters of all welding passes

Section	Welding pass	Current, I (A)	Voltage, U (V)	Welding speed, v (mm/s)	Welding efficiency, η	Heat input energy, q (kJ/mm)
S1-R	1 (back welding)	135 ~ 145	19.6	2.60	0.80	0.81 ~ 0.87
	2	180 ~ 190	21.4	4.41	0.80	0.70 ~ 0.74
S1-S	1 (back welding)	130 ~ 140	19.7	2.81	0.80	0.73 ~ 0.79
	2	185 ~ 195	21.1	3.81	0.80	0.82 ~ 0.86
S3-R	1 (back welding)	145 ~ 155	20.4	2.09	0.80	1.13 ~ 1.21
	2	200 ~ 210	23.0	4.11	0.80	0.90 ~ 0.94
	3	185 ~ 195	23.1	2.86	0.80	1.20 ~ 1.26
S3-S	1 (back welding)	160 ~ 170	20.2	2.81	0.80	0.92 ~ 0.98
	2	200 ~ 210	22.6	3.80	0.80	0.95 ~ 1.00
	3	190 ~ 200	22.8	3.35	0.80	1.03 ~ 1.09

Table 4 Key mechanical properties of S690 steel coupons

Coupon	Plate thickness (mm)	E (kN/mm^2)	f_y (N/mm^2)	f_u (N/mm^2)	ε_L (%)
Flat	6	215	733	808	15.9
Flat	10	223	754	804	17.5
Curved	10	199	838	900	12.4

Table 5 Mesh convergence study of two-dimensional models for transverse bending

Mesh	Number of layers	Global mesh size (mm)	Total number of elements	Computational time (min)	PEEQ at the inner surface (%)	Normalized transverse stress at the inner surface (/)
TB20	20	0.50	~ 5,560	2	19.4	0.643
TB50	50	0.20	~ 20,100	5	18.7	0.757
TB100	100	0.10	~ 51,000	16	17.8	0.795

Table 6 Programme and results of mesh convergence study

Mesh	Global mesh size (mm)	Local mesh size at weld groove (mm)	Number of elements			Total number of elements	Computational time (hours)	$\varepsilon_{t,in,max}$ (%)	$\varepsilon_{c,in,max}$ (%)
			through thickness	at corner	along length				
L03	6.7	3.5	3	9	66	~ 11,880	12	0.379	-0.164
L04	5.0	2.1	4	11	76	~ 23,100	31	0.389	-0.148
L06	3.3	1.4	6	16	115	~ 88,900	145	0.391	-0.115

Table 7 Investigation programme of numerical models for sequentially-coupled thermomechanical analyses

Section	Dimensions (mm)					Number of welding passes	Number of layers through thickness	Total number of elements
	t	R_{in}	B	H	L			
S1-R	6	18	150	150	560	2	3	~ 55,800
S1-S	6	18	150	150	560	2	3	~ 46,400
S3-R	10	30	200	200	760	3	4	~ 23,100
S3-S	10	30	200	200	760	3	4	~ 23,400

Table 8 Force equilibrium in Sections S3-R and S3-S

Section	Data types	Total tension force, F_T (kN)	Total compression force, F_C (kN)	Resultant force, $F_R = F_T + F_C$ (kN)	Force ratio, $f_r = \|F_R\| / \{\|F_T\| + \|F_C\|\}$ (%)
S3-R	Numerical simulation	567	-601	-34	**2.9**
	Sectioning method	246	-338	-92	**15.8**
S3-S	Numerical simulation	486	-501	-15	**1.5**
	Sectioning method	144	-240	-96	**25.0**

Table 9 Simplified longitudinal residual stresses for CFSHS

a) Sections R

Section	f_y (N/mm^2)	β
S1-R	733	-0.056
S2-R	733	-0.089
S3-R	754	-0.073
S4-R	754	-0.056

b) Sections S

Section	f_y (N/mm^2)	β_1	β_2
S1-S	733	-0.074	-0.192
S2-S	733	-0.053	-0.137
S3-S	754	-0.097	-0.253
S4-S	754	-0.074	-0.192